

17. EPICLASTIC SEDIMENTATION DURING THE UPPER MIOCENE–LOWER PLIOCENE VOLCANIC HIATUS OF GRAN CANARIA: EVIDENCE FROM SITES 953 AND 954¹

Jean-Luc Schneider,² Charlotte A. Brunner,³ and Sherry Kuttner³

ABSTRACT

The geologic history of a volcanic oceanic island is recorded in the sediments deposited in its volcanic apron, including noneruptive periods that are typically poorly represented or missing from subaerial outcrops. In this study, the history of Gran Canaria during the Gran Canaria “volcanic hiatus,” a period of volcanic quiescence from 8.3 to 4.3 Ma, is examined in detail using multiple lines of evidence from lithology, grain-size analysis, mineralogy, and micropaleontology of turbidites. Examined are Sites 953 and 954 on the north flank of the Gran Canaria apron. Sediments deposited during the late Miocene/early Pliocene noneruptive period on Gran Canaria bear a number of qualities that reflect the environment of their source. They were deposited slowly (~22 m/m.y.), because there was no active volcanism adding fresh volcanoclastic debris to island reservoirs as at other times during island development and because the surface area of the island was probably small. Turbidite structures and textures indicate transport by low-density turbidity currents, rather than high density types observed in intervals affected by active eruption. Benthic foraminifer assemblages indicate that the volcanoclastics were stored on the upper slope prior to turbidite transport to the apron, and show little influence from a shelf reservoir as do faunas from the late Pliocene and Quaternary. The composition of the clastic particles indicates that erosion dissected volcanic formations older than the volcanic hiatus, mainly the lava flows and ignimbrites of the Fataga Group and the basaltic shield of Gran Canaria. We infer the rapid formation of deep barrancos during the geomorphological evolution of the island when volcanic activity was absent. Active volcanism returned during the latest part of the “volcanic hiatus” at ~5.5 Ma in the form of submarine hydroclastic basaltic activity (pre-Roque Nublo volcanic phase), marked by the presence of hydroclastic particles and by a change in the composition of the clinopyroxenes of the sand fraction.

INTRODUCTION

During the evolution of volcanoes, eruptive phases are short-lived events that correspond to the main constructional phases of volcanic edifices. However, erosion during noneruptive periods is also important to the morphologic history of the volcano. Weathering and erosion of volcanic formations strongly dissect volcanic edifices and produce large quantities of epiclastic material. Erosion rates can be high in volcanic successions mainly because volcanic glass is metastable and, consequently, very sensitive to weathering. Volcanic epiclastic particles can suffer strong morphological maturation during sedimentary transit and, in so doing, leave a record of erosion intensity. Erosion rates are dependent, in part, on the climate, but mainly on the effusive or pyroclastic nature of the volcanic material; for instance, unwelded pyroclastic deposits are highly erodible. As erosion rates can be very high, the downslope transportation of the volcanic epiclastic material to the volcanoclastic apron surrounding the volcanic domain is rapid. Epiclastic processes in volcanic provinces are still poorly understood.

One of the objectives of Leg 157 was to study the characteristics of offshore sedimentation during a long noneruptive period in the evolution of the oceanic island of Gran Canaria. This main period of volcanic quiescence is called the “upper Miocene–lower Pliocene volcanic hiatus of Gran Canaria” (Lietz and Schmincke, 1975; Schmincke, 1994). The purpose of this investigation is to describe the main sedimentological, mineralogical, and paleontological characteristics of the epiclastic sediments deposited on the northern flank of

the submarine volcanoclastic apron of Gran Canaria (Sites 953 and 954) and to infer from this data the geologic history of the island during the volcanic hiatus, which is very poorly represented in land-based sequences.

Volcanological Evolution of Gran Canaria and its Record in the Apron

The evolution of the alkaline province of the Canary Islands (Schmincke, 1976, 1982; Schmincke and von Rad, 1979) has been connected to the Canaries hot spot since the Upper Cretaceous (Schmincke, 1994). The magmatic and volcanic evolution of the emergent portion of Gran Canaria is well constrained for the last 15 m.y., based on studies of land-based volcanic sequences (Schmincke, 1969, 1976, 1982, 1994; McDougall and Schmincke, 1977). The subaerial growth of the island began with emergence of shield basalts ~15 Ma; followed by ~0.7 m.y. of volcanism that produced the silicic pyroclastic flows of the Mogán Group (14.1–13.4 Ma; van den Bogaard et al., 1988); and followed by the ash flows, lava flows, and fallout tephra of the Fataga Group between ~13.4 and 9.5 Ma. The Fataga Group includes a large trachytic-monolithic cone sheet swarm in the central caldera complex injected near the end of this eruptive period. The quiescent volcanic hiatus followed the Fataga events and was concluded by eruption of the Roque Nublo Group from ~5 to 3.4 Ma (Pérez-Torrado et al., 1995). Eruptions of undersaturated lava flows continued between 3.2 and 1.7 Ma at rates much slower than those of the Roque Nublo events, and a small amount of volcanism has continued on Gran Canaria during the Quaternary in a region restricted to the northeastern half of the island.

The volcanic apron that surrounds Gran Canaria has developed throughout growth of the subaerial volcanic edifice. The apron consists of large volumes of volcanoclastic sediments (Menard, 1956), and comprises ~90% of the total volume of the island including both submarine and subaerial parts. Sites 953 and 954 penetrate proximal and distal locales on the north edge of the apron (Fig. 1), and varia-

¹Weaver, P.P.E., Schmincke, H.-U., Firth, J.V., and Duffield, W. (Eds.), 1998. *Proc. ODP, Sci. Results, 157*: College Station, TX (Ocean Drilling Program).

²Université des Sciences et Technologies de Lille, Département des Sciences de la Terre, CNRS-URA 719, Bâtiment S.N.5, 59655 Villeneuve d'Ascq cedex, France. Jean-Luc.Schneider@univ-lille1.fr

³University of Southern Mississippi, Institute of Marine Sciences, John C. Stennis Space Center, MS 39529, U.S.A.

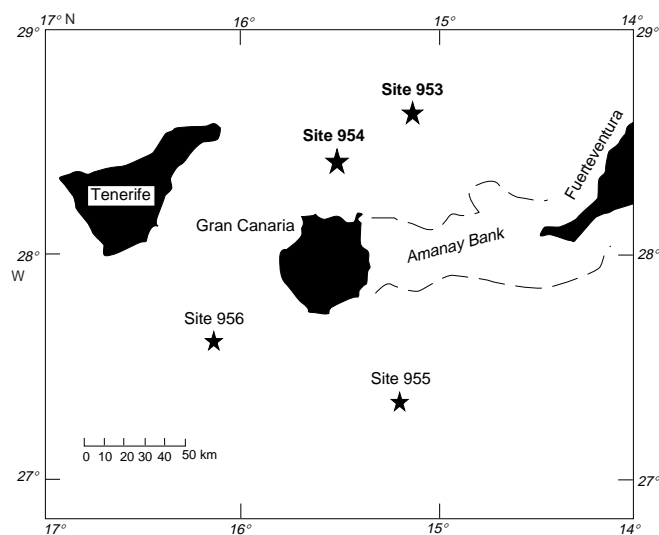


Figure 1. Locations of the drilling sites on the submarine volcaniclastic apron of Gran Canaria.

tions of sedimentation rates in the holes (Fig. 2) directly reflect the volcanic evolution of the island. The highest sedimentation rates correspond to the times of emplacement of thick basaltic hyaloclastites and lapillistones during the middle Miocene shield stage of the island. These deposits are overlain at Sites 953, 955, and 956 by volcaniclastic turbidites that correlate to the thick subaerial pyroclastic flow deposits of the Mogán and the Fataga groups. The main hiatus in volcanic activity of Gran Canaria (9.6–4.4 Ma) corresponds to a period of intense erosion, which is reflected by comparatively low volcaniclastic input to the apron. Most recent volcaniclastic deposits of the apron (4.5–0 Ma, basaltic and tephritic volcaniclastic turbidites) record the youngest phase of volcanic activity (Roque Nublo Group).

The Upper Miocene–Lower Pliocene Volcanic Hiatus

The main volcanic hiatus (8.3–4.3 Ma, Shipboard Scientific Party, 1995a; 9.6–4.4 Ma, Lietz and Schmincke, 1975) is a major period of volcanic quiescence, during which the island underwent strong erosion. This erosion led to major dissection of the volcanic edifice, a conclusion supported by the absence of sediments between the Fataga and Roque Nublo groups. In the central part of the island, the lava flows and debris avalanche deposits of the Roque Nublo Group overlie unconformably the cone sheet dike swarm of the Fataga group in the central part of the Tejada caldera (Schmincke, 1994). Thin braided fluvial deposits are, however, intercalated into the unconformity surface. The fluvial deposits reflect the erosion and transport of the epiclastic material from the central part of the island toward the sea. Outside the central caldera, deep canyons (barrancos) carve the volcanic pile of the emergent domain of the island and lead to reworking of a wide spectrum of volcanic detritus.

The northern flank of the submarine apron is an ideal location for studying the record of the epiclastic sedimentation during the volcanic hiatus. The basin north of Gran Canaria is isolated from clastic influx from the western African margin by a submarine topographic high, the Amanay Bank (Fig. 1), between Gran Canaria and Fuerteventura (Funck, 1995). Consequently, clastic sediments deposited at Sites 953 and 954 during the “volcanic hiatus” probably come from Gran Canaria. This assumption is confirmed by the absence of quartz within the sedimentary record in contrast to its abundance on the southern flank of the apron where large volumes of clastic mate-

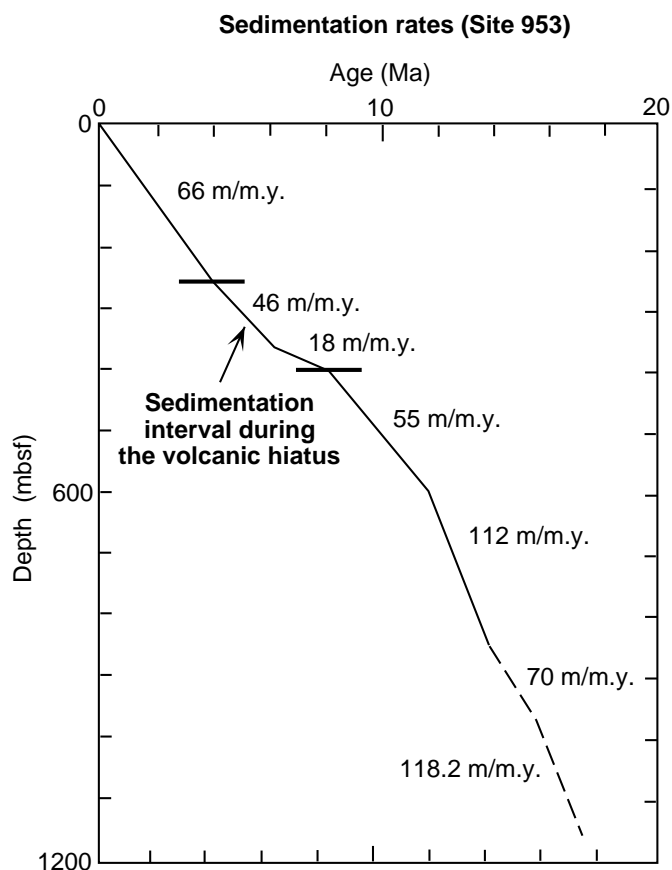


Figure 2. Sedimentation rates, Site 953 (from Shipboard Scientific Party, 1995a).

rial derived from the African continent were deposited (Sites 955 and 956; Goldstrand, Chap. 20, this volume).

Deposits equivalent to the erosional interval were recovered from Leg 157 sites. Clastic sedimentation occurred on the submarine apron during the main noneruptive period in the volcanic activity on Gran Canaria, and the deposits have been recognized at Site 953 from Section 157-953C-10R-1 through 23R-6. This interval corresponds to lithostratigraphic Unit III (264–398 meters below seafloor [mbsf] at this site (Shipboard Scientific Party, 1995a; Fig. 3). The equivalent interval at Site 954 extends from Section 157-954B-11R-2 through 35R-1 (179–408 mbsf) and also corresponds to lithostratigraphic Unit III (Shipboard Scientific Party, 1995b). These units are characterized by a low influx of volcaniclastic material in comparison with periods of intense volcanic activity, despite the fact that large volumes of volcanic material were eroded from the island during the late Miocene to early Pliocene (several hundred cubic kilometers; Schmincke, 1994). The deposits, which reflect the strong erosion of Gran Canaria, consist of thin and low-frequency volcaniclastic silt and sand layers interlayered with pelagic sediments (nannofossil oozes).

Nomenclature of the Volcaniclastic Particles

The terminology used in this report is from Fisher (1961, 1966). The term “volcaniclastic” is defined to include the entire spectrum of clastic materials composed in part or entirely of volcanic fragments, formed by any particle-forming mechanism (e.g., pyroclastic, hydroclastic, epiclastic, and autoclastic), transported by any mechanism, deposited in any physiographic environment or mixed with any other

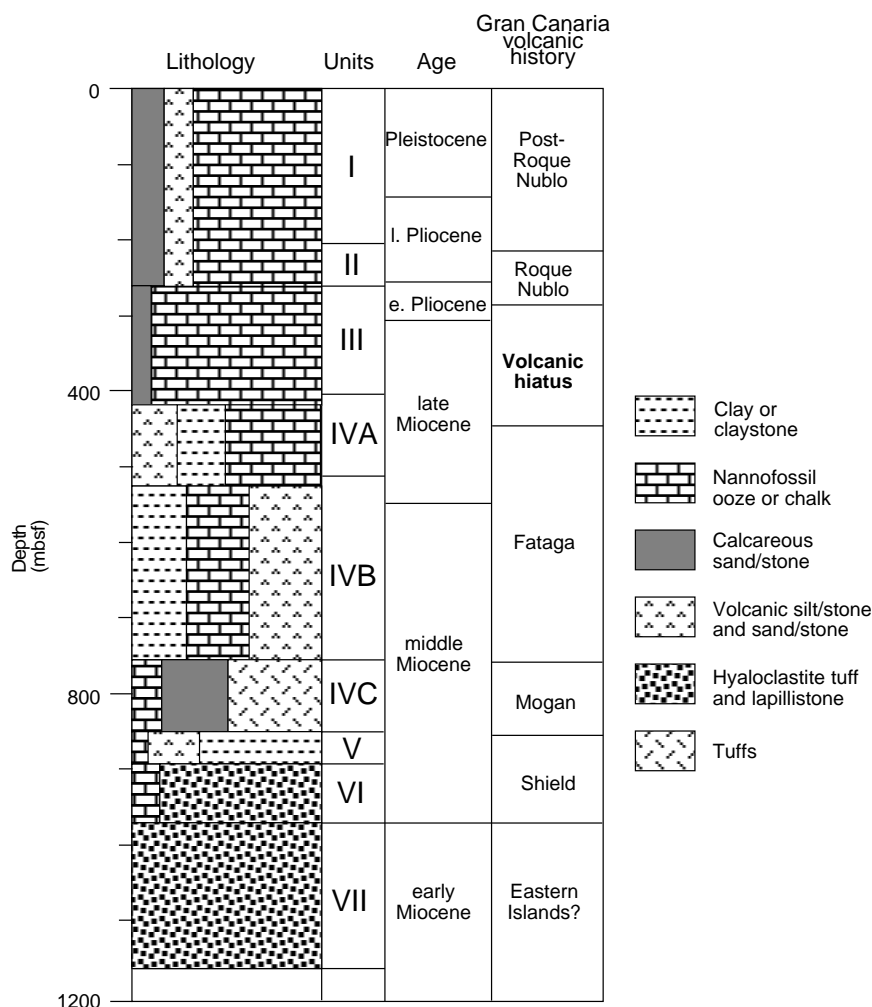


Figure 3. Lithostratigraphy of Site 953 (from Shipboard Scientific Party, 1995a).

volcaniclastic type or with any nonvolcanic fragment type in any proportion (Fisher, 1966; Fisher and Schmincke, 1984; Fisher and Smith, 1991). Among volcaniclastics, epiclastic particles are lithic clasts and crystals derived from any type of pre-existing rock by weathering and erosion. If the pre-existing rocks are volcanic, the epiclasts are considered one type of volcaniclastic particle (i.e., volcanic epiclasts). Pyroclastic and hydroclastic particles reworked by rivers, wind, or other types of transporting agents, are not designated epiclastic because they were not formed by weathering but are considered as reworked pyroclastic or hydroclastic particles.

METHODS

Sedimentological, grain size, mineralogical, and paleontological analyses were done on samples from Sites 953 and 954. Most of the analyses concern samples from Site 953, because Unit III is more complete and less disturbed by slumping than at Site 954. Depositional sequences were observed by means of macroscopic observations on wet, split cores.

As the grain size of the samples was always <2 mm and samples were poorly consolidated, we analyzed the granulometric distributions of 41 sand and silt samples from Units I and III and Subunit IVA of Site 953 and 33 samples from Units I and III of Site 954 with a laser diffraction granulometer (Malvern Ltd., Loizeau et al., 1994) at University of Lille. Each sample was disaggregated in water for 2 min and ultrasonicated for 10 s. The procedures and formulas used to

obtain textural parameters from grain-size analysis are those of Folk and Ward (1957) and Folk (1974). These parameters are the mean graphic size and the sorting index.

Samples were air dried and then sieved by hand to recover the sand fraction. Because of the preservation of the turbiditic sequences, only sand concentrates from Site 953 (35 samples) were impregnated with epoxy resin on glass slides and thin-sectioned.

Mineral compositions of bulk rocks and clay minerals from the <2- μ m fraction (128 samples from Site 953; 60 samples from Site 954) were examined by X-ray diffraction (XRD) at the Laboratoire de Sédimentologie et Géodynamique, University of Lille. Holtzapfel (1985) summarizes preparation of the samples and analytical conditions.

Counts of 600 grains/sample were done on the sand fraction of 21 samples selected from the base to the top of the volcanic hiatus interval in Site 953. Table 1 displays the surface percentages of the different kinds of particles.

Minerals (mainly pyroxenes and amphiboles) and glass shards from 16 samples from Unit III (Site 953) were analyzed for major elements on a CAMEBAX SX 50 microbeam electron microprobe combined with an energy-dispersive analytical system (EDS) at the CAMPARIS Microanalytical Center at the Université Pierre et Marie Curie, Paris. Analytical settings were 15 kV and 10 nA, and counting times were 10 to 20 s for all major elements. Under these conditions, concentrations <0.1 wt% are considered unreliable. Na and Si were analyzed simultaneously and first. Mineral standards were albite for Na; orthoclase for K and Al; diopside for Si, Ca, and Mg; synthetic

Table 1. Point-count data of clastic sediments of the volcanic hiatus (Unit III), Hole 953C.

Core, section, interval (cm)	Depth (mbsf)	Unit/ Subunit	Major components			Lithic fragments				Monomineralic grains							Total points	
			Biogenic	Lithic	Monomineralic grains	Basaltic glass (fresh)	Basaltic glass (altered)	Basalt	Trachyphonolite	Alkali feldspar	Clinopyroxene	Amphibole	Biotite	Titanite	Zeolite	Opaque		
157-953C-																		
9R-3, 58-60	257.28	II	8	79	13	21	0	33	25	2	10	1	0	0	0	0	0	600
10R-1, 84-86	264.54	III	66	14.5	19.5	tr.	0	3.5	11	9	6.5	2.5	1	0	0	0	0.5	600
10R-3, 74-78	267.44	III	63	10.5	26.5	0	0	0.5	10	14	3.5	5	2.5	1	0	0	0.5	600
11R-2, 144-148	276.34	III	75.5	12	12.5	5	0	5	2	3.5	5	3.5	0.5	0	0	0	tr.	600
11R-4, 90-94	278.80	III	76	15.5	8.5	0.5	0	7	8	1	3	3.5	tr.	0	0	0	1	600
14R-2, 23-25	304.13	III	27	54.5	18.5	5	0	9	40.5	6	10	1.5	0.5	0	0	0	0.5	600
15R-1, 20-23	312.30	III	60	31.5	8.5	1	0	1	29.5	3.5	4	0.5	0	0	0	0	0.5	600
15R-1, 94-96	313.04	III	17	72	11	48.5	0	18.5	5	3.5	7	0.5	0	0	0	tr.	tr.	600
15R-1, 100-105	313.10	III	21	69.5	9.5	50.5	0	16	3	4.5	5	tr.	0	0	0	tr.	tr.	600
15R-1, 107-111	313.17	III	6	79	15	52.5	0	21.5	5	3	11.5	0.5	0	0	0	tr.	tr.	600
16R-1, 20-21	321.80	III	59.5	28	12.5	3	0	4	21	3	7.5	1	tr.	0	0	0	1	600
18R-2, 72-74	342.82	III	27	42.5	30.5	11.5	0	12.5	18.5	16.5	5.5	1.5	tr.	0	7	tr.	tr.	600
19R-1, 97-99	351.17	III	27	47.5	25.5	0	1.5	4	42	10	12	1.5	tr.	0	0	0	2	600
19R-2, 40-43	352.10	III	30	53	17	0	3	8	42	5	11	tr.	tr.	0	0	0	1	600
20R-2, 32-34	361.62	III	34.5	55	10.5	0	0.5	9	45.5	4	4	1	0	0.5	0	0	1	600
21R-4, 71-73	376.21	III	6.5	82	11.5	0	1	14	67	5	4.5	1.5	0	0	0	0	0.5	600
22R-1, 97-99	380.07	III	52	37	11	0	3	7	27	4	6.5	0.5	0	0	0	0	tr.	600
22R-3, 89-91	382.99	III	37.5	49.5	13	0	15.5	19	15	7	5	0.5	0.5	0	0	0	tr.	600
22R-5, 80-82	385.90	III	32	54.5	13.5	0	0.5	7	47	8.5	3	1	tr.	0	0	0	1	600
24R-4, 2-4	402.62	IVa	8	67.5	24.5	0	0	1	66.5	21	3	0.5	0	0	0	0	tr.	600
25R-2, 27-29	409.47	IVa	28	50	22	0	2	5	43	7	12.5	1.5	tr.	0	0	0	1	600

Fe₂O₃ for Fe; synthetic Cr₂O₃ for Cr; synthetic MnTiO₃ for Mn and Ti; and synthetic NiO for Ni. All synthetic minerals were obtained from the Bureau de Recherches Géologiques et Minières.

Turbidite samples were selected for micropaleontologic examination from the Miocene to early Pliocene interval coeval with the volcanic hiatus and from the Late Pliocene and Quaternary interval above the Roque Nublo deposits. It is interesting to compare the two intervals because both are deposited during periods of relative volcanic inactivity. Samples were washed in a sieve with 63- μ m openings and sieved again when dry on a screen of 150- μ m openings. Benthic foraminifers were separated from mineral-rich sands by heavy liquid flotation and from fossil-rich sands by hand picking under a binocular dissecting microscope. Samples with >300 specimens were used with confidence because they are sensitive (significantly >0) to frequencies >2% at the 95% confidence level (Patterson and Fishbein, 1989). Some samples contained as few as 100 benthic foraminifers, so these samples were used with less confidence and are sensitive to only 9% at the 95% confidence level (Patterson and Fishbein, 1989). A few samples contain <100 specimens, and these were used with great caution and only in support of interpretations made from samples with more specimens.

The benthic foraminifers were identified to genus and species where possible and classified into depth zones according to the published depth preference of each taxon on the northwest African continental margin (Lutze, 1980; Lutze and Coulbourn, 1984; Haake, 1980; Mathieu, 1971, 1988; Murray, 1991). In this work, we grouped together species with similar depth ranges into depth assemblages. We found six assemblages useful for interpretation of paleodepth because they have restricted depth ranges (Table 2) and six assemblages not useful for interpretation of paleodepth; one because the taxa have unknown depth preferences, and five because the taxa have very broad depth preferences (Table 2).

Another faunal measure of paleodepth was used. We examined changes in benthic foraminifer suborders in the late Miocene to Pleistocene (Table 3; Fig. 4). Three suborders dominate the fauna, *Rotalina*, *Miliolina*, and *Textulariina*. The *Rotalina* have shells made of low-magnesian calcite and dominate bathyal environments; *Miliolina* have shells made of high-magnesian calcite and are most abundant and diverse in neritic environments, especially in environments starved of clastic detritus; and *Textulariina* have shells made of agglutinated sand and silt grains and are most abundant and diverse in neritic environments and at great abyssal depths below the calcium carbonate compensation depth.

DESCRIPTION OF THE DEPOSITIONAL SEQUENCES

Sequences

Dark fine sand and silt layers of the hiatus generally occur as thin millimeter- to centimeter-scale, graded or planar laminated sequences. Grading is often missing, and lamination is marked by color changes that are related to the relative foraminifer content of the laminae. Current-ripple lamination is rare in the deposits, whereas planar lamination is more usual. Very thin layers (<0.3 mm) are sometimes disturbed by vertical burrows (Pl. 1, Fig. 1). Load-casted ripples at the bases of silty deposits are present in Section 157-953C-21R-5 (Pl. 1, Fig. 2). The bases of the sequences are sharp and tops generally diffuse. The thin clastic sequences are overlain by decimeter- to meter-thick, carbonate-rich hemipelagic intervals that are usually strongly bioturbated.

In Section 157-953C-15R-1, an 18-cm-thick dark layer occurs (Pl. 1, Fig. 3). The sequence displays grading and planar lamination. The top of the sequence is a 4-cm-thick silty layer, which could correspond to the fallout deposit of fine-grained material elutriated during the turbiditic flow before emplacement. This turbidite sequence

is constituted by 70% basaltic material (glass shards and basaltic clasts, see below) and could correspond to a primary volcanoclastic deposit.

Soft-Sediment Deformation

Some intervals of Unit III at Sites 953 and 954 are strongly affected by soft-sediment deformation, which is characteristic of this non-eruptive period on Gran Canaria. At Site 953, slumped sediments occur mainly from 321 to 388 mbsf, and at Site 954, in the interval from 302 to 359 mbsf. However, as indicated by fauna hiatuses (Shipboard Scientific Party, 1995b), slumping was certainly more important at Site 954, which is located in a more proximal and probably steeper part of the volcanoclastic apron. Folds and small faults were recognized, and stretched and boudinated silty layers are present within some fold structures. In some places, brecciation affects the deposits (Pl. 1, Fig. 4), breaking them into rounded clasts, 1–5 cm in size. In some sections, the turbidite layers are completely mixed with calcareous hemipelagic sediments (nannofossil oozes and chalks). In these levels, volcanoclastic lithic fragments and crystals are dispersed within the calcareous sediments. Small-scale folds are sometimes related to these structures, suggesting that the mixing is related to soft-sediment deformation which induces liquefaction of the sediments.

DESCRIPTION OF THE SEDIMENTS

Grain-Size Analysis

At Site 953, grain-size data of clastic sediments from Unit III have been compared with Subunit IVA and Unit I (Table 4), whereas at Site 954 they have been compared with Unit I (Table 5). Clastic sediments deposited during the "volcanic hiatus" are mainly siltstones (Fig. 5) containing various amounts of very fine to fine sand particles (up to 25%; Table 4). Sorting varies in both sites from 1.50 to 2.60, indicating the poorly sorted character of the clastic sediments. Apparently, the sorting of the turbidite sands is independent on the mean graphic size (Fig. 6). This characteristic is probably also related to the presence of foraminifer tests. At Site 953 and 954, sands of Unit I are coarser than sediments of Unit III. This characteristic could be related to the fact that volcanoclastic sediments of Unit I are directly dependent on volcanic activity and rapidly reworked into the basin, whereas mobilization of Unit III sediments is only related to weathering and erosion during the "volcanic hiatus." However, turbidites from Subunit IVA (Fataga Group) at Site 953 display the same grain-size characteristics as those of Unit III sediments (Fig. 6A).

Petrography of the Sand Fraction

Sand fractions from the turbiditic sequences and from mixed sediments with scattered lithics and crystals always contain large proportions of foraminifers (6%–59.5%), mainly planktonic foraminifers. The micritic matrices of the turbidite layers observed in thin sections always contain large proportions of coccoliths. All these calcareous biogenic components were probably picked up from the seafloor during flow of the turbiditic currents. Crystals and lithics are always present, but in small proportions. In Table 1, we report the results of modal analysis (Site 953). For comparison, we studied one sample from Unit II and two samples from Subunit IVA.

Among the lithics, basalt and trachyonolite dominate. Lithic fragments are always subrounded to rounded, and their morphology suggests abrasion during fluvial sedimentary transport on land. Sample 157-953C-9R-3, 58–60 cm, from Unit II is richer in lithic fragments (79%) than sediments of Unit III. Fragments of trachyonolitic ignimbrites of the Fataga Group are commonly observed (Pl. 2, Fig. 1), and rounded trachyonolite lava fragments are ubiquitous (Pl. 2, Fig. 2). Alkaline syenite clasts were observed (Sections 157-

Table 2. Benthic foraminifer taxa by depth zone.

Depth sensitive assemblages		
Shelf 0-130 m	Shelf-upper bathyal 0-1000 m	Upper bathyal 130-1000 m
<i>Astronion stellagera</i> discorbids <i>Hanzawaia</i> <i>Hanzawaia concentrica</i> <i>Heterolepa</i> <i>Neocorbina terquemi</i> <i>Neoponides schreiberi</i> <i>Quinqueloculina</i>	<i>Ammoglobigerina</i> <i>Angulogerina forasini</i> <i>Bolivina</i> cf. <i>B dilatata</i> <i>Bulimina gibba</i> <i>Bulimina striata</i> <i>Cibicides lobatulus</i> <i>Elphidium</i> <i>Elphidium complanata</i> <i>Gaudryina</i> <i>Gavelinopsis</i> cf. <i>G. praegeri</i> <i>Heterolepa</i> sp. B <i>Nonionella</i> <i>Trifarina</i>	<i>Angulagerina bradyi</i> <i>Angulogerina elongatastrata</i> <i>Bolivina subaenariensis</i> <i>Cibicides refulgens</i> <i>Cibicidoides pseudoungeriana</i> <i>Ehrenbergina undulata</i> <i>Melonis barleeaanum</i> <i>Paromalina coronata</i> <i>Planulina arimenensis</i> <i>Uvigerina auberiana</i>
Middle bathyal 1000-2000 m	Upper-middle bathyal 130-2000 m	Lower bathyal-abyssal 2000->3000 m
<i>Gyroidina zelandica</i> <i>Osangularia</i> cf. <i>O. culter</i>	<i>Pullenia quinqueloba</i>	<i>Melonis pompilioides</i> <i>Signavirgulina tortuosa</i>
Depth insensitive assemblages		
Upper-lower bathyal 130-3000 m	Upper bathyal-abyssal 130->3000 m	Middle bathyal-abyssal 1000->3000 m
<i>Bulimina striata mexicana</i> <i>Eilohedra</i> <i>Eilohedra quiqueloba</i> <i>Oridorsalis</i> <i>Uvigerina peregrina</i>	<i>Fontbotia wuellerstorfi</i> <i>Nuttalides</i> <i>Oridorsalis tener</i> <i>Oridorsalis umbonatus</i> <i>Sphaeroidina bulloides</i>	<i>Bulimina alazanensis</i> <i>Cibicides robersonianus</i> <i>Gyroidina orbicularis</i> <i>Gyroidina soldanii</i> <i>Laticarinina</i> <i>Pullenia bulloides</i>
Shelf-middle bathyal 0-2000 m	Shelf-bathyal 0-3000 m	Unknown depth preference
<i>Bolivina pseudo-plicata</i> <i>Trifarina angulosa</i>	<i>Articulana</i> fragment <i>Bolivina</i> <i>Brizalina</i> <i>Cassidulina</i> <i>Cibicides</i> <i>Cibicidoides</i> <i>Cibicidoides bradyi</i> <i>Cibicidoides mundala</i> <i>Egerella</i> <i>Epistominella</i> <i>Globocassidulina</i> <i>Gyroidina</i> <i>Lenticulina</i> <i>Melonis</i> <i>Melonis affinis</i> <i>Pullenia</i> sp. A	<i>Anomalina</i> <i>Bolivina</i> sp. <i>Osangularia</i> <i>Pleurostomella</i> <i>Polystomella</i> <i>Recouvigerina</i> <i>Reussella</i> <i>Siphonina</i> (ridges) <i>Siphonina tubulosa</i> <i>Stilostomella</i> <i>Valvulinaria</i> cibicidids unknowns lagenids miliolids nodosarids

Note: Depth measured as water depth in meters.

953C-21R-4 and 22R-3). These clasts are very similar to the syenites, which are present in the Miocene cone sheet dike swarm within the Tejada caldera (intrusions of the Tejada Formation; Schmincke, 1967, 1994; Ferriz and Schmincke, 1989). Basaltic fragments always display an oxide-rich groundmass and commonly contain olivine pseudomorphs (Pl. 2, Fig. 3). Quenched plagioclase microliths are present in some basaltic clasts. These basaltic fragments probably come from the basaltic shield of Gran Canaria.

In Section 157-953C-15R-1, the black 20 cm-thick graded bed (Pl. 1, Fig. 3) contains >90% brown glass shards. Rare tachylitic shards contain delicate plagioclase microliths. The vesicles of these glass particles are often filled by clay minerals (smectites), and glass, even if it looks fresh, is always slightly birefringent. The shards are blocky and slightly vesicular, suggesting hydroclastic fragmentation. Completely weathered brown glass particles are present from Section 157-953C-22R-5 through 19R-1.

Monomineralic grains are dominantly alkali feldspars (up to 16.5%) and clinopyroxenes (up to 11.5% in Unit III), with less amounts of amphiboles (up to 3.5%) and biotite (up to 2.5%). Clinopyroxenes occur as crystal fragments in the sand fraction of the turbidite layers. Rounded crystals are relatively rare because of their small size, but cockscomb dissolution structures on edges were often observed. Clinopyroxene looks optically fresh, and some crystals

contain small acicular undetermined inclusions. Titanite occurs in Samples 157-953C-10R-3, 74–76 cm, and 22R-5, 80–82 cm. Quartz was never observed.

Figure 7 presents the plots of component proportions of the clastic deposits vs. depth. Abundance of trachyphonolitic clasts decreases slightly from bottom to top of Unit III, whereas basaltic clasts and clinopyroxene crystals become more abundant. Samples from Section 157-953C-15R-1 are very rich in basaltic material and correspond to the black thick volcanoclastic turbidite layer. Decreasing proportions of trachyphonolitic clasts suggest rapid erosion of the lavas and tuffs of the Fataga Formation so that the basaltic shield was quickly reached.

Mineralogy of the Clastic Sediments

X-ray Diffractometry of Bulk-Rock and Clay Fraction

We analyzed all samples (turbidite layers and hemipelagic sediments) by XRD analysis. All samples are very rich in calcite because of the high proportion of foraminifers and coccoliths. No samples contain quartz in the silt and sand fractions. The absence of quartz is probably because of the presence of the Amanay Bank between the islands of Gran Canaria and Fuerteventura, which forms a sill against all turbiditic clastic influx from the northwestern African margin.

Table 3. Proportions of benthic foraminifer specimens in each bathymetric zone in 15 turbidites, Site 953.

Core, section, interval (cm)	Unit	Depth (mbsf)	0-130 (m)	0-1000 (m)	130-1000 (m)	0-2000 (m)	130-2000 (m)	1000-2000 (m)	130-3000 (m)
157-953A-									
12H-3, 28-30	I	105.89	6.0	37.6	25.6	0.4	1.6	0.0	1.6
16H-3, 5-7	I	143.66	15.4	26.9	3.8	0.0	0.0	0.0	0.0
18H-5, 132-134	I	166.93	9.1	15.2	15.2	9.1	3.0	0.0	0.0
157-953C-									
6R-1, 36-38	II	225.87	12.5	17.9	12.5	0.0	0.0	0.0	1.8
10R-3, 74-78	III	267.46	5.7	1.9	11.3	0.0	3.8	1.9	1.9
11R-2, 144-148	III	276.36	0.0	0.0	0.0	0.0	0.0	0.0	0.0
15R-1, 20-22	III	312.31	5.0	0.0	45.0	0.0	0.0	0.0	5.0
15R-1, 100-102	III	313.11	6.0	4.0	42.0	0.0	0.0	0.0	0.0
18R-4, 58-61	III	345.70	4.5	2.6	46.1	3.2	1.3	3.2	4.5
19R-1, 97-99	III	351.18	2.6	22.5	70.4	0.0	0.0	0.8	0.0
20R-2, 12-14	III	361.43	10.2	7.8	44.1	0.3	0.6	3.1	1.6
22R-3, 89-91	III	383.00	5.7	12.2	39.6	0.8	0.8	2.4	3.5
24R-2, 129-131	IV	400.90	0.0	14.3	14.3	0.0	0.0	0.0	14.3
26R-4, 11-13	IV	421.92	0.0	7.1	35.7	0.0	0.0	7.1	0.0
31R-2, 145-148	IV	468.46	5.1	14.1	44.2	0.0	0.0	0.6	2.6

Notes: Depth measured as water depth in meters. Indet. = indeterminate.

Table 3 (continued).

Core, section, interval (cm)	Unit	Depth (mbsf)	0-3000 (m)	130-3000 (m)	1000-3000 (m)	2000-3000 (m)	Indet.	Total tests
157-953A-								
12H-3, 28-30	I	105.89	12.8	2.0	1.2	0.8	10.4	250.0
16H-3, 5-7	I	143.66	19.2	3.8	0.0	26.9	3.8	26.0
18H-5, 132-134	I	166.93	21.2	6.1	0.0	6.1	15.2	33.0
157-953C-								
6R-1, 36-38	II	225.87	16.1	7.1	0.0	3.6	28.6	56.0
10R-3, 74-78	III	267.46	24.5	3.8	9.4	3.8	32.1	53.0
11R-2, 144-148	III	276.36	100.0	0.0	0.0	0.0	0.0	2.0
15R-1, 20-22	III	312.31	15.0	0.0	0.0	0.0	30.0	20.0
15R-1, 100-102	III	313.11	26.0	2.0	4.0	4.0	12.0	50.0
18R-4, 58-61	III	345.70	17.5	2.6	0.0	1.3	13.0	161.0
19R-1, 97-99	III	351.18	2.1	0.0	0.0	0.0	1.6	614.0
20R-2, 12-14	III	361.43	12.4	5.6	1.6	1.2	11.5	331.0
22R-3, 89-91	III	383.00	12.2	0.3	1.1	2.2	19.2	372.0
24R-2, 129-131	IV	400.90	14.3	0.0	0.0	14.3	28.6	7.0
26R-4, 11-13	IV	421.92	21.4	0.0	0.0	0.0	28.6	14.0
31R-2, 145-148	IV	468.46	3.8	0.0	3.8	0.0	25.6	156.0

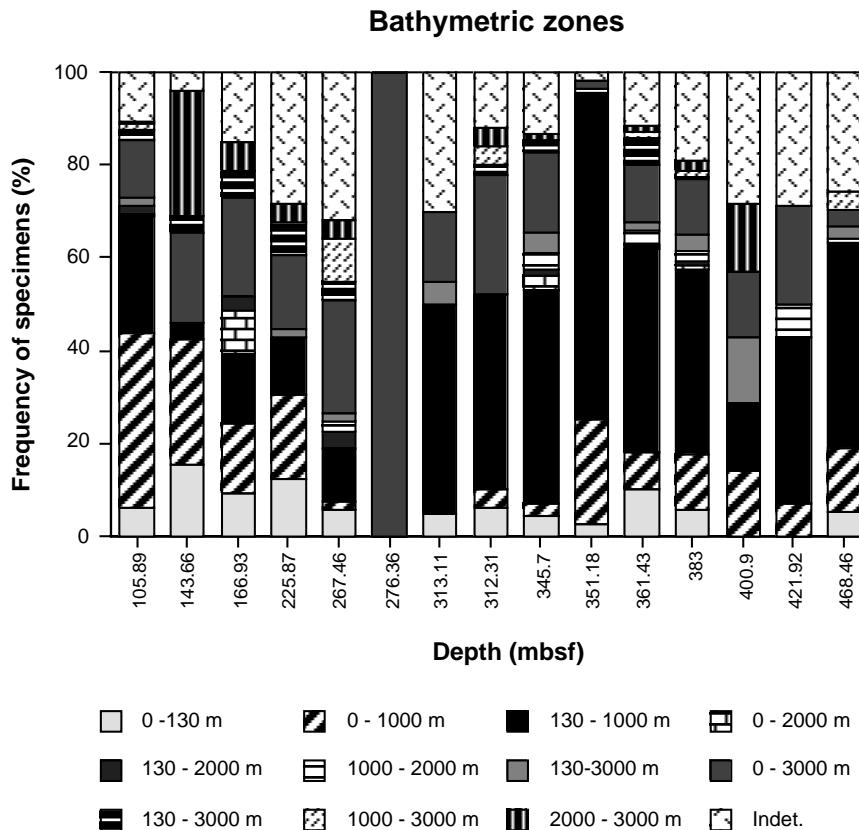


Figure 4. Stacked bar graph showing percentages of specimens in each bathymetric zone in 15 turbidites from Site 953. Note that samples below 264 mbsf are dominated by a depth assemblage limited to upper bathyal depths (130–1000 m), whereas samples above 264 mbsf are dominated by both the upper bathyal assemblage (130–1000 m) and one with broader environmental preferences that ranges from the shelf to upper bathyal depths (0–1000 m).

Table 4. Grain-size characteristics of the clastic deposits of Unit I and Unit III (volcanic hiatus), and Subunit IVA, Site 953.

Core, section, interval (cm)	Unit/Subunit	Petrography	Graphic mean	Sorting index	Phi 95	Phi 84	Phi 50	Phi 16	Phi 5	Clay	Silt	Very fine sand	Fine sand	Medium sand	Coarse sand	Very coarse sand
157-953A-																
1H-3, 130-132	I	Volcanic sand with calcareous components	3.66	2.50	8.97	6.64	2.85	1.49	0.97	3.80	27.90	14.90	25.30	22.40	5.60	0.00
6H-1, 41-43	I	Black volcanic sand	3.25	2.18	7.64	5.97	2.43	1.35	0.86	0.20	26.40	11.00	25.60	29.50	7.10	0.20
12H-3, 28-30	I	Black volcanic sand	4.01	1.51	7.64	5.64	3.57	2.81	2.38	1.60	34.70	39.60	22.50	1.50	0.10	0.00
16H-3, 5-7	I	Black volcanic sand	3.98	1.30	7.64	5.16	3.74	3.04	2.59	1.90	36.90	46.20	14.00	0.90	0.00	0.00
16H-6, 28-30	I	Volcanic sand with calcareous components	3.21	1.60	7.38	4.92	2.68	2.02	1.60	0.20	22.50	15.50	46.60	14.60	0.60	0.00
18H-5, 132-134	I	Black volcanic sand	4.18	1.44	7.64	5.72	3.79	3.04	2.60	1.80	40.50	42.90	13.90	0.90	0.00	0.00
157-953C-																
10R-1, 84-88	III	Nannofossil chalk with lithic grains	7.71	2.05	9.97	9.97	7.77	5.38	4.01	25.80	69.40	4.60	0.30	0.00	0.00	0.00
10R-2, 82-84	III	Nannofossil chalk with lithic grains	7.18	1.84	9.97	8.97	7.42	5.16	4.11	21.30	74.70	3.80	0.10	0.00	0.00	0.00
10R-3, 74-78	III	Silty foraminifer nannofossil chalk with crystals	7.56	2.08	9.97	9.97	7.50	5.21	4.08	22.70	73.00	4.10	0.20	0.00	0.00	0.00
11R-2, 144-148	III	Nannofossil chalk with amphibole crystals	7.79	1.88	9.97	9.97	7.62	5.80	4.44	23.60	74.30	2.20	0.00	0.00	0.00	0.00
11R-4, 90-94	III	Nannofossil chalk with black crystals	7.85	1.88	9.97	9.97	7.70	5.88	4.29	25.10	71.70	3.00	0.10	0.00	0.00	0.00
12R-2, 24-25	III	Coarse-grained crystal lithic siltstone	7.37	2.18	9.97	9.97	7.31	4.84	4.04	20.60	74.80	4.50	0.10	0.00	0.00	0.00
13R-1, 13-15	III	Siltstone	7.01	1.84	9.97	8.97	6.96	5.11	4.21	13.40	83.40	2.90	0.30	0.00	0.00	0.00
13R-4, 84-87	III	Clayey nannofossil mixed sediment with lithics	8.09	1.61	9.97	9.97	7.91	6.38	5.27	28.10	71.80	0.10	0.00	0.00	0.00	0.00
13R-5, 51-52	III	Nannofossil chalk with crystals	5.45	1.86	8.97	7.64	5.01	3.70	3.17	5.60	70.30	21.00	3.00	0.00	0.00	0.00
14R-2, 23-25	III	Lithic siltstone	6.25	2.07	9.97	8.38	6.29	4.08	3.38	10.60	75.30	12.20	1.90	0.00	0.00	0.00
15R-1, 20-23	III	Foraminifer lithic siltstone	7.70	1.95	9.97	9.97	7.56	5.57	4.32	21.20	76.10	2.60	0.10	0.00	0.00	0.00
15R-1, 94-96	III	Lithic sandy siltstone	5.72	1.77	9.12	7.67	5.39	4.09	3.35	5.90	80.20	11.50	2.30	0.10	0.00	0.00
15R-1, 100-105	III	Lithic sandy siltstone	5.40	1.86	9.06	7.48	5.01	3.72	3.03	5.50	72.00	17.70	4.50	0.20	0.00	0.00
15R-1, 107-111	III	Lithic sandy siltstone	5.60	1.80	9.03	7.62	5.23	3.93	3.21	5.40	77.40	13.90	3.10	0.20	0.00	0.00
16R-1, 20-22	III	Clayey nannofossil chalk with lithic sand	6.21	1.80	9.97	7.97	6.15	4.51	3.80	7.80	85.00	6.50	0.70	0.00	0.00	0.00
16R-3, 28-30	III	Lithic crystal siltstone	7.08	1.88	9.97	8.97	7.25	5.01	4.08	16.80	79.00	3.90	0.30	0.00	0.00	0.00
17R-1, 13-15	III	Lithic siltstone	7.97	1.80	9.97	9.97	7.88	6.06	4.51	26.80	71.30	1.90	0.00	0.00	0.00	0.00
18R-2, 72-74	III	Lithic crystal sandy siltstone	5.68	1.88	8.97	7.97	5.23	3.86	3.32	8.70	71.40	18.10	1.80	0.00	0.00	0.00
18R-CC, 16-18	III	Lithic calcareous sandy siltstone	5.87	2.27	9.97	8.38	5.68	3.54	2.95	11.70	62.30	20.30	5.60	0.10	0.00	0.00
19R-1, 97-99	III	Crystal sandy siltstone	6.25	2.56	9.97	8.97	6.60	3.17	2.61	12.40	63.10	10.80	13.70	0.00	0.00	0.00
20R-4, 33-35	III	Foraminifer lithic siltstone with crystals	6.75	2.03	9.97	8.97	6.76	4.54	3.88	14.60	79.20	5.70	0.50	0.00	0.00	0.00
21R-2, 74-76	III	Nannofossil clayey mixed sedimentary rock with crystals	6.65	2.16	9.97	8.97	6.76	4.21	3.54	12.50	75.60	10.80	1.10	0.00	0.00	0.00
21R-5, 108-110	III	Lithic crystal siltstone	7.01	1.94	9.97	8.97	7.19	4.88	3.92	17.10	77.30	5.00	0.60	0.00	0.00	0.00
22R-4, 22-24	III	Lithic crystal siltstone	7.94	1.77	9.97	8.97	7.81	6.06	4.72	27.10	71.20	1.50	0.10	0.00	0.00	0.00
23R-1, 39-41	III	Claystone with nannofossil with lithic crystal base	6.94	1.91	9.97	8.97	6.93	4.92	4.04	14.10	81.20	4.20	0.50	0.00	0.00	0.00
24R-3, 15-17	IVA	Crystal lithic sandy siltstone	6.43	1.95	9.97	8.38	6.48	4.44	3.59	9.40	81.30	8.10	1.30	0.00	0.00	0.00
25R-1, 17-19	IVA	Siltstone	7.07	1.83	9.97	8.97	7.15	5.11	4.24	16.70	80.40	2.70	0.20	0.00	0.00	0.00
25R-1, 105-107	IVA	Mixed sedimentary rock with silt	7.09	1.73	9.97	8.97	6.97	5.32	4.54	13.70	84.90	1.40	0.10	0.00	0.00	0.00
25R-2, 56-58	IVA	Claystone with sandy base	5.81	1.65	9.97	7.64	5.52	4.27	3.68	4.60	85.70	9.00	0.80	0.00	0.00	0.00
25R-4, 65-67	IVA	Silty claystone	6.91	1.88	9.97	8.97	6.81	4.97	4.18	13.40	83.30	3.10	0.30	0.00	0.00	0.00
26R-1, 39-41	IVA	Mixed sedimentary rock with lithics	7.24	1.74	9.97	8.97	7.37	5.38	4.41	20.40	77.60	1.90	0.10	0.00	0.00	0.00
26R-3, 125-127	IVA	Crystal siltstone	6.89	1.86	9.97	8.97	6.75	4.97	4.26	13.50	83.90	2.40	0.20	0.00	0.00	0.00
27R-1, 147-150	IVA	Lithic crystal siltstone	6.32	1.55	8.97	7.97	6.23	4.76	4.04	6.90	88.50	4.10	0.50	0.00	0.00	0.00
27R-2, 128-130	IVA	Crystal lithic siltstone with foraminifers	5.83	1.80	8.97	7.97	5.44	4.08	3.47	5.80	80.30	12.40	1.40	0.00	0.00	0.00
28R-2, 79-80	IVA	Crystal lithic siltstone	6.29	1.82	8.97	8.97	6.18	4.32	3.68	8.50	82.00	8.80	0.70	0.00	0.00	0.00

Table 5. Grain-size characteristics of the clastic deposits of Unit I and Unit III (volcanic hiatus), Site 954.

Sample	Unit	Petrography	Graphic mean	Sorting index	Phi 95	Phi 84	Phi 50	Phi 16	Phi 5	Clay	Silt	Very fine sand	Fine sand	Medium sand	Coarse sand	Very coarse sand
157-954A-																
3H-3, 140-142	I	Volcanic sand with calcareous components	1.46	1.18	4.69	2.43	1.39	0.55	0.03	0.00	5.90	3.50	17.00	40.80	28.00	4.70
6H-1, 88-90	I	Volcanic sand with calcareous components	1.85	0.90	4.25	2.60	1.82	1.14	0.71	0.00	5.30	4.10	30.60	48.70	10.80	0.40
6H-5, 136-138	I	Dark volcanic sand	3.21	2.25	7.57	6.14	2.22	1.26	0.75	0.20	21.70	7.30	29.00	32.50	9.10	0.30
10H-2, 63-65	I	Dark volcanic silt	6.24	1.84	9.54	8.31	5.97	4.44	3.82	9.30	83.50	6.60	0.60	0.00	0.00	0.00
157-954B-																
12R-3, 2-4	III	Lithic crystal sandy siltstone	5.96	2.00	9.30	8.14	5.83	3.92	3.05	7.50	75.30	12.60	4.30	0.30	0.00	0.00
13R-CC, 18-21	III	Nannofossil chalk with lithics	7.35	1.92	10.46	9.31	7.38	5.38	4.27	20.40	76.50	2.90	0.30	0.00	0.00	0.00
15R-1, 18-20	III	Siltstone	7.21	1.72	9.90	8.92	7.27	5.45	4.28	15.40	81.70	2.70	0.30	0.00	0.00	0.00
15R-2, 85-87	III	Siltstone	6.51	1.77	9.69	8.36	6.40	4.76	3.99	10.00	85.00	4.50	0.50	0.00	0.00	0.00
16R-1, 5-7	III	Nannofossil chalk with lithic grains	7.14	1.62	9.99	8.76	7.07	5.57	4.58	13.70	84.70	1.50	0.20	0.00	0.00	0.00
18R-2, 47-52	III	Nannofossil chalk with black crystals	7.69	1.93	10.73	9.59	7.74	5.75	4.34	23.90	73.40	2.60	0.10	0.00	0.00	0.00
20R-1, 122-124	III	Siltstone	7.00	1.98	10.31	9.11	6.96	4.92	4.16	17.60	78.90	3.20	0.20	0.00	0.00	0.00
21R-1, 12-14	III	Crystal lithic siltstone	7.61	1.89	10.66	9.53	7.57	5.74	4.43	22.80	75.20	2.00	0.00	0.00	0.00	0.00
21R-5, 8-9	III	Nannofossil chalk with black crystals	7.38	2.00	10.54	9.39	7.49	5.26	4.13	21.20	75.00	3.70	0.10	0.00	0.00	0.00
22R-1, 9-12	III	Nannofossil chalk with black crystals	7.86	1.72	10.61	9.55	7.85	6.17	4.82	24.90	73.90	1.10	0.00	0.00	0.00	0.00
24R-2, 92-94	III	White sandy siltstone	6.56	1.95	9.47	8.56	6.70	4.40	3.47	10.60	79.00	8.50	1.90	0.10	0.00	0.00
26R-3, 42-46	III	Nannofossil mixed sediment with lithics	6.75	1.75	9.57	8.53	6.83	4.88	4.03	10.50	84.80	4.20	0.40	0.00	0.00	0.00
27R-1, 55-59	III	Nannofossil mixed sediment with lithics	7.38	1.74	10.31	9.14	7.36	5.63	4.61	18.40	80.20	1.40	0.10	0.00	0.00	0.00
27R-6, 30-34	III	Nannofossil chalk with black crystals	7.41	1.70	10.27	9.08	7.42	5.72	4.58	17.40	80.80	1.70	0.10	0.00	0.00	0.00
28R-1, 120-122	III	Lithic crystal siltstone	7.17	1.73	10.22	8.92	7.15	5.43	4.56	15.40	83.30	1.30	0.00	0.00	0.00	0.00
28R-1, 140-142	III	Lithic crystal siltstone	6.88	1.71	9.80	8.63	6.88	5.14	4.29	11.90	85.30	2.50	0.30	0.00	0.00	0.00
28R-2, 19-21	III	Siltstone	6.69	1.82	9.69	8.60	6.69	4.78	4.01	11.40	83.70	4.40	0.50	0.00	0.00	0.00
28R-2, 89-91	III	Lithic crystal siltstone	6.85	1.78	10.01	8.66	6.84	5.04	4.23	12.60	84.20	2.90	0.30	0.00	0.00	0.00
29R-1, 82-84	III	Lithic crystal siltstone	5.95	1.72	9.10	7.79	5.74	4.32	3.51	5.90	83.80	8.50	1.90	0.00	0.00	0.00
29R-4, 84-86	III	Claystone with crystals and lithics	6.61	1.80	9.44	8.48	6.69	4.67	3.87	9.80	84.00	5.60	0.60	0.00	0.00	0.00
30R-1, 2-18	III	Siltstone	7.00	1.71	9.94	8.75	6.99	5.26	4.38	13.30	84.50	2.10	0.20	0.00	0.00	0.00
30R-1, 85-86	III	Siltstone	6.73	1.81	9.79	8.61	6.75	4.84	4.05	11.80	83.70	4.10	0.40	0.00	0.00	0.00
30R-2, 54-56	III	Silty claystone with lithics and crystals	7.63	1.72	10.59	9.46	7.51	5.93	5.04	22.10	77.50	0.40	0.00	0.00	0.00	0.00
30R-3, 78-80	III	Crystal lithic sandy siltstone	6.35	1.89	9.43	8.45	6.22	4.39	3.69	9.70	81.50	7.90	0.90	0.00	0.00	0.00
30R-4, 74-76	III	Crystal lithic siltstone	6.84	1.68	9.94	8.63	6.68	5.20	4.50	12.30	86.30	1.30	0.10	0.00	0.00	0.00
30R-5, 38-40	III	Crystal lithic sandy siltstone	5.50	1.88	8.85	7.52	5.32	3.66	2.80	4.40	74.00	14.60	6.30	0.70	0.00	0.00
30R-5, 75-77	III	Mixed sedimentary rock	6.91	1.81	10.10	8.76	6.88	5.08	4.25	13.80	83.30	2.70	0.30	0.00	0.00	0.00
31R-1, 93-95	III	Crystal lithic sandy siltstone	5.67	1.84	8.99	7.69	5.47	3.87	3.19	5.20	76.30	15.40	3.10	0.10	0.00	0.00
31R-4, 46-48	III	Crystal lithic siltstone	6.15	1.78	9.41	8.12	5.93	4.41	3.80	8.00	84.50	6.90	0.60	0.00	0.00	0.00

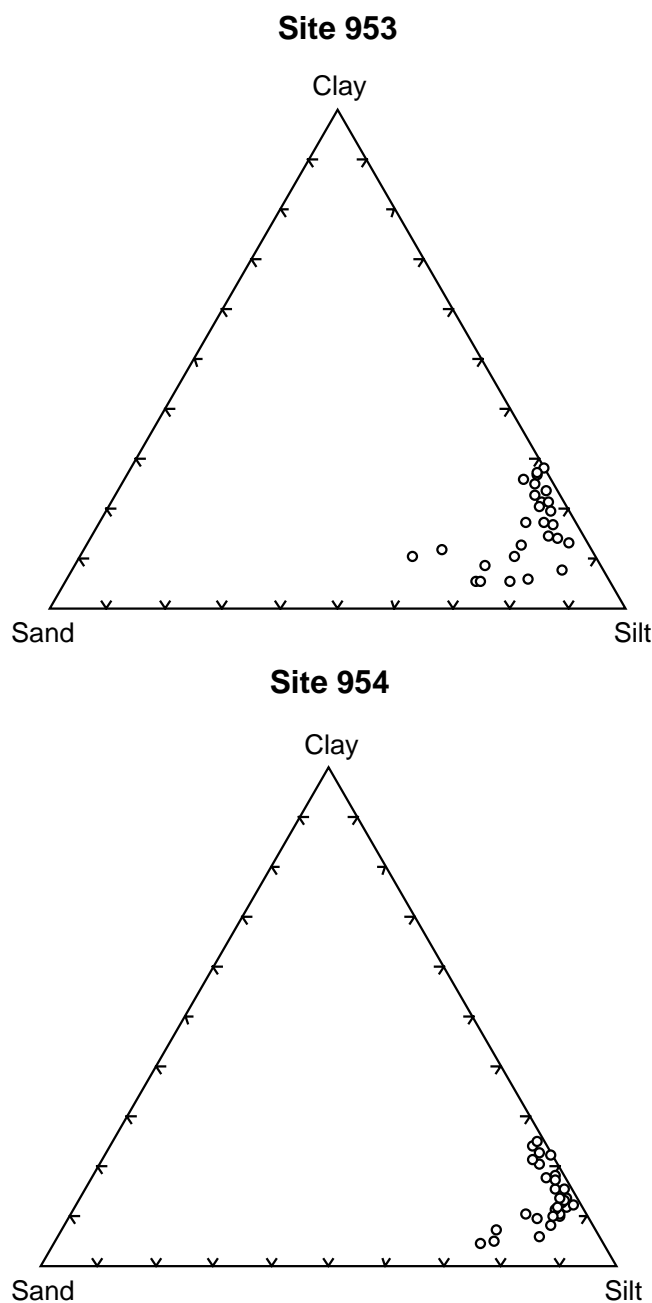


Figure 5. Triangular plots of grain-size fractions in the turbidites of the volcanic hiatus sequence, Sites 953 and 954.

Consequently, most of the clastic material recovered at Sites 953 and 954 must be derived only from Gran Canaria. Only some silt-size material could be of eolian origin.

The study of the clay fraction of the pelagic claystones and of the matrix of the turbidites did not yield significant results, because the matrix is mainly calcitic (nanofossils) and the clay mineral content is very low. Semiquantitative analysis of clay mineral abundance reveals that smectite and chlorite are the most abundant clay minerals. Unfortunately, these semiquantitative data do not allow a study of climatic changes at the source areas of the clastic material. The smectite content is higher during Subunit IVA deposition than during the "volcanic hiatus," probably reflecting the weathering of the volcanic material (mainly glass; Chamley, 1986) on the subaerial part of Gran Ca-

naria and after submarine emplacement on the volcanoclastic apron. The smectite content increases upcore from Core 157-953C-15R. For instance, the clay fraction of the black volcanoclastic turbidite layer (Sample 157-953C-15R-1, 87–114 cm) contains 100% smectite altered from the abundant basaltic brown glass particles in this layer.

Microprobe Analysis of the Sand Fraction

During microprobe analysis of minerals in 16 thin sections of the sand fraction, clinopyroxenes, as well as amphiboles and hydroclastic vitroclasts, were systematically analyzed. Clinopyroxenes from Subunit IVA have also been analyzed for comparison.

Clinopyroxenes

Only the cores of grains were analyzed in this study to avoid the effect of weathering of crystals rims and to allow comparisons between individual crystals from individual layers. Zoning of the crystals and alteration on edges of the crystal fragments was always weak. Representative clinopyroxenes analyses are reported in Table 6. The clinopyroxenes analyzed correspond mainly to salite in the Ca-Mg-(Fe_{tot} + Mn) diagram (Poldervaart and Hess, 1951; Fig. 8). Some plots fall in the fields of diopside, endiopside, and augite.

To distinguish different categories within the clinopyroxenes, we have established variation diagrams based on major-element contents of clinopyroxene structural formulas. The structural formulas have been calculated on the basis of six oxygens. Element contents in clinopyroxenes are dependent on the crystallization conditions (White, 1964; Wass, 1979). For instance Al IV, Ti, Na, and the Mg number (Mg/Mg + Fe) are good markers of genetic affinities between individual crystals mixed in epiclastic sediments and their possible sedimentary sources.

Figure 9 represents the composition variations of the clinopyroxenes by intervals within the volcanic hiatus sequence. At the base of the hiatus, most of the clinopyroxenes display a common genetic relationship characterized by a linear correlation (Na-Ti and Al IV-Ti diagrams). From Core 157-953C-15R to the top of the hiatus interval, results are more scattered, indicating the appearance of a new category of clinopyroxenes in the deposits (Fig. 9). This new group of clinopyroxenes probably comes from another igneous source. The structural formulas from analyses of clinopyroxenes from Mogán and Fataga Groups on the island (Crisp and Spera, 1984; Fig. 10) indicate that the evolutionary trends of the Mogán and Fataga Groups clinopyroxenes differ from the trend of the clinopyroxenes recovered in Unit III at Site 953. However, analyses of clinopyroxenes of the basaltic shield of Gran Canaria (Heuschkel, 1996; Table 7; Fig. 10) strongly suggest a cogenetic relationship with the Unit III clinopyroxenes (Figs. 9, 10). Consequently, most of the clinopyroxene crystals in the turbiditic layers deposited during the volcanic hiatus are derived from the Miocene basaltic shield of Gran Canaria.

Amphiboles

Amphiboles are present in all the turbidites, but their amount is very small. When present, amphiboles were systematically analyzed by microprobe. Structural formulas on the basis of 24 oxygens were established, and the amphibole type determined using the Leake (1978) classification. Representative compositions are given in Table 8.

Most amphiboles are calcic and titaniferous (kaersutite, pargasite, and hastingsite). Rare low-Ti calcic (tschermarkite) and sodic-calcic amphiboles have been analyzed (richterite). No significant changes in amphibole compositions are observed from the base to the top of Unit III at Site 953. However, kaersutite seems to be more abundant toward the top. These amphiboles could originate from either the Mogán or Fataga volcanic intervals of Gran Canaria.

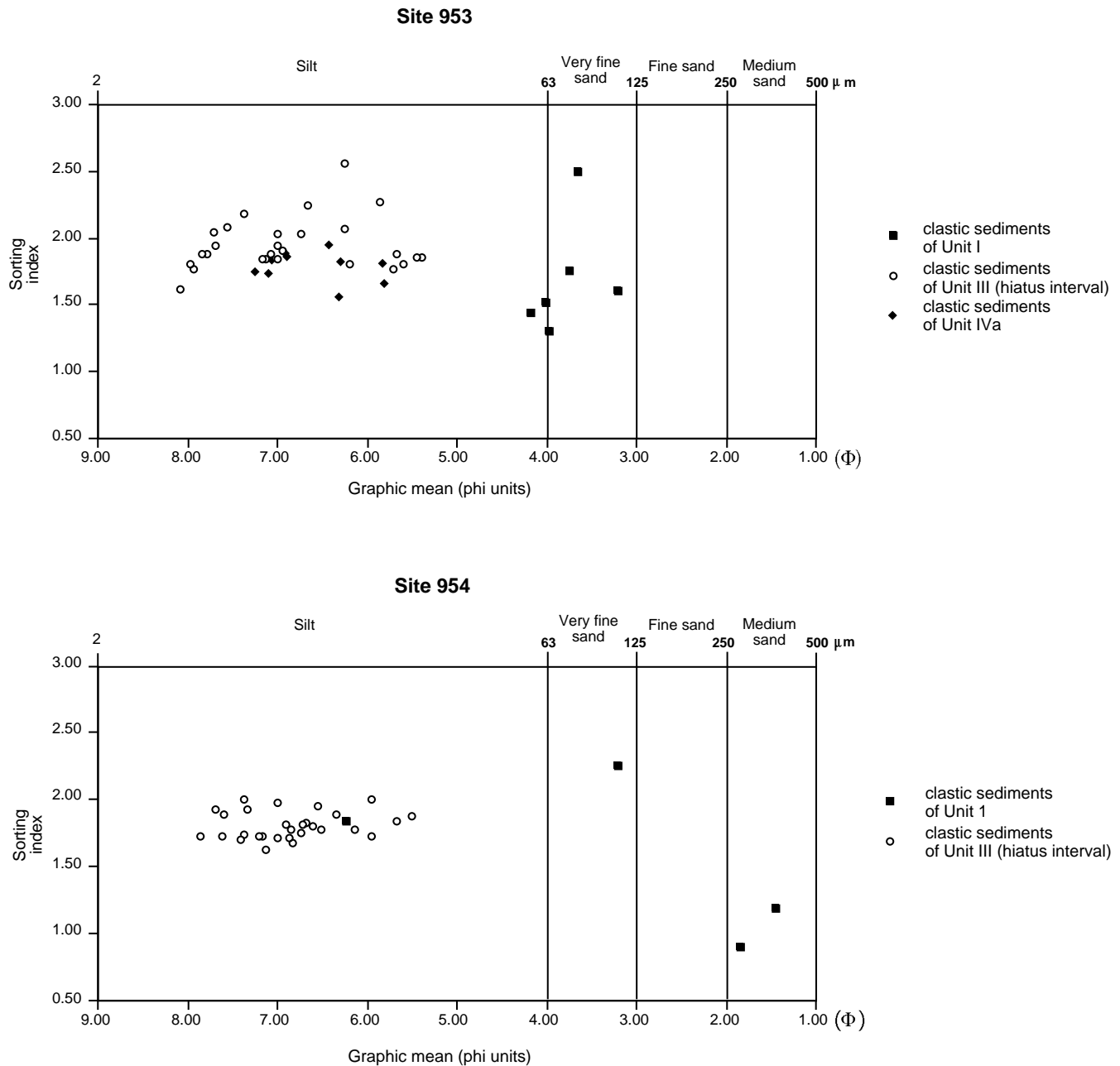


Figure 6. Relationships between the sorting index and the graphic mean of the clastic sediments of the volcanic hiatus and comparison with data of the enclosing units for Sites 953 and 954.

Biotites

We observed few biotite crystals in all sand fractions, and they are present from the base to the top of Unit III in Site 953. Biotite is typical of the Fataga Group volcanic rocks. Its appearance marks the base of this interval on Gran Canaria (ignimbrite F; Gerbe and Schmincke, 1996).

Feldspars

Most of the feldspars from the clastic sediments of the hiatus at Site 953 are alkalic (65% Ab, 30% Or, and 5% An, on average), however, rare plagioclase (An₄₈₋₅₇) was observed. Evolution of the feld-

spar composition does not display an upward trend in Unit III at Site 953. Consequently, feldspars cannot be used as source markers in these epiclastic formations, because they can be derived from all older volcanic formations.

Glass Shards

Glass shards are very rare in the turbiditic sediments of Unit III except in Section 157-953C-15R-1. In this section, we investigated the black volcanoclastic turbidite layer, which contains ~90% glass. Because of hydration and alteration to smectitic clay minerals, microprobe analyses did not produced convincing results. The best analysis has an oxide sum of 80% and the composition of the glass is basaltic.

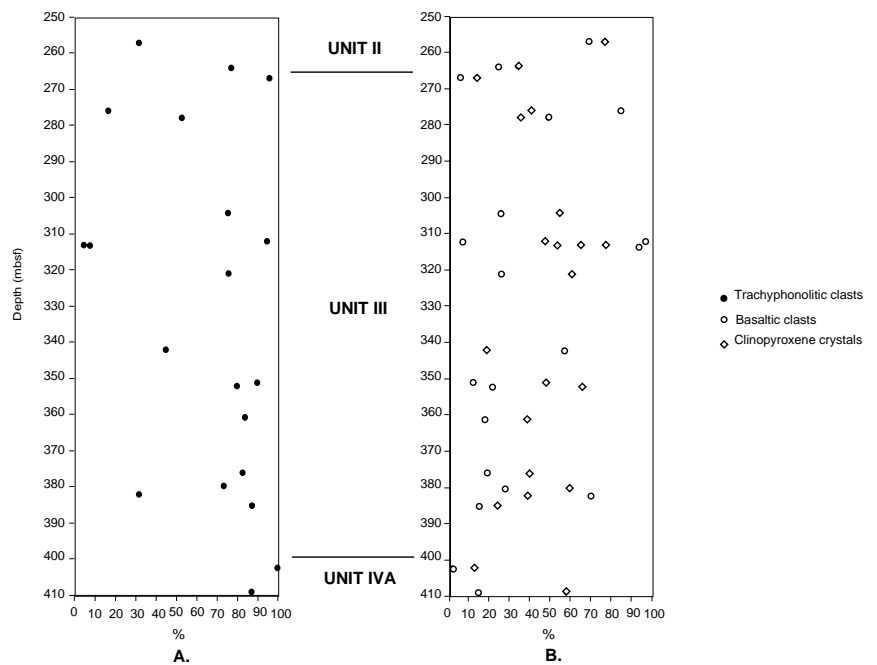


Figure 7. **A.** Variations of trachyphonolitic clasts among the lithic clasts content of Unit III sediments vs. depth, Site 953. **B.** Variations of basaltic clasts and clinopyroxene crystals content of the “volcanic hiatus” sediments

Benthic Foraminifer Assemblages

Volcaniclastic-rich turbidites from the late Miocene through the Quaternary are dominated by two benthic foraminifer assemblages from the upper bathyal depth zone: one assemblage from 130 to 1000 m that consists of taxa limited to the upper slope and another assemblage from 0 to 1000 m that includes taxa ranging throughout the shelf and the upper slope. Other specimens reworked into the samples include a small number of specimens that belong to other depth restricted assemblages from neritic, middle bathyal and lower bathyal to abyssal depths (Table 2); as many as 20% that belong to depth insensitive assemblages (Table 2), and the remainder that have unknown depth preferences or are unidentified because of poor preservation (Table 2). In the late Miocene to early Pliocene interval, the bathyal assemblage from 130 to 1000 m dominates and the assemblage from 0–1000 m is subordinate. By contrast, after termination of the Roque Nublo eruptive period in the late Pliocene, the bathyal assemblage from 0 to 1000 m becomes dominant and the one from 130 to 1000 m becomes subordinate.

Another turbidite assemblage appears in the late Pliocene and Quaternary that is not seen at all in the volcanic hiatus interval. Neritic biogenic carbonate turbidites first appear in the late Pliocene interval at ~215 mbsf, and become thicker and more frequent in the Pleistocene. The turbidites contain abundant *Miliolina* (>10%) and *Textulariina* (>5%) compared to volcaniclastic turbidites (Table 9; Fig. 11; biogenic carbonate turbidites from 3.88, 9.32, 31.89, 70.88, 115.27, and 149.80 mbsf), suggesting a neritic source on a clastic-starved shelf. This interpretation is supported by the co-occurrence of abundant bryozoans, pelecypods, and gastropods characteristic of temperate carbonate bryozoan reefs that grow on open marine shelves with restricted clastic input.

DISCUSSION

Sedimentation Rates During the Volcanic Hiatus Interval

Sedimentation rates on the submarine volcaniclastic apron were minimal during the upper Miocene–lower Pliocene “volcanic hiatus.” At Site 953, the average sedimentation rate during the hiatus interval is 35 m/m.y. (40 m/m.y. at Site 954). This is ~10 times less than

during deposition of Subunit IVA, which is contemporaneous with the Fataga volcanic phase on Gran Canaria (335 m/m.y.). This strongly suggests that reworking of volcaniclastic material is rapid during eruptive periods.

Characteristics of the Sedimentation

The characteristics of clastic depositional sequences (thin deposits, paucity of current-ripple lamination, presence of load-casted ripples) suggest that sediments were deposited mainly by low-density turbidity currents (Mutti, 1992) during the upper Miocene–lower Pliocene “volcanic hiatus” on the submarine volcaniclastic apron north of Gran Canaria. Bottom currents also could have controlled the deposition of some clastic layers. Moreover, thin amalgamated planar-laminated sequences similar to very thin traction carpets (Shanmugam et al., 1993), and the frequent absence of grading in the deposits suggest turbiditic flows that are continuous during a relatively long period. Such turbidity currents could be related to floods of fluvial systems in the subaerial areas (Durringer et al., 1991). This hypothesis is supported by the small volume of the turbidites that were probably not linked to large slump events at the submarine flanks of Gran Canaria. Such large slumps initiating turbiditic currents were certainly active during eruptive periods as is probably the case when turbidity currents rapidly emplaced volcaniclastic material.

In spite of moderate core recovery for Unit III at Sites 953 (61%) and 954 (56.5%), we suggest that the thickness of turbidite beds, their low-density character, and the very low proportion of turbidites compared to hemipelagic calcareous deposits are related to the relatively small subaerial surface area of the island and wide dispersal of the epiclastic material on the apron. The clastic influx is only controlled by erosion active in the subaerial part of Gran Canaria.

The soft-sediment deformation of the hiatus-related sediments is related to slope destabilization after deposition. We do not invoke slope instabilities caused by sediments overloading during the volcanic hiatus interval because of low sedimentation rates during this period. However, the beginning of a new phase of volcanic activity on Gran Canaria ~5.5 Ma (pre-Roque Nublo or Roque Nublo volcanic phase upcore of Section 157-953C-15R-1) could have induced instability a long time after deposition of the sediments on the apron. This hypothesis is supported by brecciation of partly indurated sediments

Table 6. Representative compositions of clinopyroxenes in the silts and sands of Unit III, Site 953.

Core, section, interval (cm):	10R-1, 84-86	10R-3, 74-76	11R-2, 144-146	12R-1, 6-8	14R-2, 23-25	15R-1, 20-22	15R-1, 20-22	15R-1, 107-109	15R-1, 107-109
SiO ₂	45.88	43.27	46.34	52.84	47.66	44.11	50.92	49.52	50.87
TiO ₂	2.48	3.23	2.78	0.66	2.27	4.42	1.43	1.57	1.45
Al ₂ O ₃	6.80	8.13	6.23	2.24	5.82	8.44	3.19	4.87	3.15
Cr ₂ O ₃	0.04	0.06	0.02	1.11	0.12	0.08	0.33	0.99	0.44
FeO	10.13	12.01	9.66	4.26	6.87	7.77	7.04	5.70	6.50
MnO	0.19	0.25	0.47	0.07	0.13	0.13	0.25	0.10	0.10
NiO	0.08	0.00	0.00	0.10	0.00	0.01	0.01	0.05	0.05
MgO	10.48	8.85	10.75	16.50	13.64	11.25	15.67	15.26	16.10
CaO	22.80	22.57	22.07	22.67	22.31	22.97	21.34	21.87	21.13
Na ₂ O	0.74	0.95	1.02	0.41	0.59	0.56	0.38	0.37	0.33
Total	99.61	99.33	99.33	100.86	99.40	99.74	100.55	100.31	100.12
% Wo	50.19	50.77	49.12	46.27	47.72	51.30	43.70	45.92	43.41
% En	32.08	27.69	33.28	46.84	40.58	34.93	44.64	44.56	46.00
% Fs	17.73	21.53	17.60	6.89	11.70	13.77	11.66	9.52	10.59
Mg number	0.648	0.566	0.665	0.874	0.779	0.721	0.799	0.827	0.815
Al IV	0.247	0.318	0.229	0.078	0.211	0.329	0.122	0.173	0.122
Al VI	0.059	0.054	0.051	0.018	0.047	0.047	0.016	0.039	0.015
Ti + Cr	0.072	0.096	0.080	0.050	0.067	0.128	0.049	0.073	0.053
Ca + Na	0.989	1.011	0.979	0.913	0.940	0.973	0.870	0.891	0.859
State	Fresh crystal core	Rounded crystal core	Fresh crystal core	Fresh crystal core					

Note: The structural formulas were calculated on the basis of six oxygens.

Table 6 (continued).

Core, section, interval (cm):	16R-1, 20-22	18R-2, 72-74	19R-1, 97-99	19R-1, 97-99	19R-2, 40-42	20R-2, 32-34	21R-4, 71-73	22R-5, 80-82	22R-5, 80-82
SiO ₂	46.98	48.80	50.58	48.82	50.25	43.66	44.19	49.59	44.70
TiO ₂	2.49	2.45	1.20	2.14	1.35	3.49	3.13	1.73	3.32
Al ₂ O ₃	6.76	4.76	3.06	4.79	3.28	8.93	9.00	3.45	8.25
Cr ₂ O ₃	0.03	0.12	0.61	0.08	0.46	0.00	0.00	0.48	0.01
FeO	7.74	7.81	5.85	7.64	6.93	9.49	10.51	6.50	7.53
MnO	0.19	0.07	0.08	0.16	0.07	0.27	0.29	0.02	0.24
NiO	0.12	0	0.04	0.10	0.03	0.16	0.03	0.00	0.04
MgO	12.40	13.31	14.93	13.76	15.12	10.46	9.91	14.94	11.69
CaO	22.24	21.78	22.76	22.17	20.96	22.85	22.64	22.25	22.82
Na ₂ O	0.72	0.53	0.27	0.53	0.42	0.68	0.72	0.37	0.52
Total	99.67	99.63	99.37	100.19	98.86	100.00	100.42	99.32	99.11
% Wo	48.69	46.90	47.27	46.77	44.17	50.75	50.48	46.23	50.55
% En	37.77	39.85	43.12	40.38	44.32	32.32	30.72	43.19	36.01
% Fs	13.54	13.25	9.61	12.85	11.51	16.93	18.80	10.57	13.44
Mg number	0.741	0.752	0.820	0.762	0.795	0.663	0.627	0.804	0.734
Al IV	0.232	0.171	0.115	0.178	0.117	0.336	0.319	0.145	0.302
Al VI	0.068	0.039	0.019	0.032	0.027	0.066	0.084	0.007	0.068
Ti + Cr	0.072	0.072	0.052	0.063	0.052	0.100	0.089	0.063	0.095
Ca + Na	0.950	0.931	0.929	0.925	0.872	0.984	0.976	0.919	0.967
State	Fresh crystal core								

in Unit III. Slumped sediments are concentrated within a critical 63 m-thick sequence in the sedimentary pile at Site 953 (330–396 mbsf) and a 127-m-thick sequence at Site 954 (235–362 mbsf).

Provenance of the Volcaniclastic Material

The eroded and weathered character of the clastic material is suggested by rounding and alteration of mineral and lithic grains. The angularity of the clasts of younger deposits contrasts with the more mature character of deposits contemporaneous with the “volcanic hiatus.” Modal analysis of clastics (lithic fragments and monomineralic crystals) of Unit III at Site 953 indicates that they were eroded from older volcanic formations of Gran Canaria (Miocene basaltic shield, Mogán and Fataga Groups). The Fataga Group was eroded throughout the whole volcanic hiatus as indicated by reworking of trachypholitic clasts. Epiclastic particles eroded from the Mogán Group have not been clearly recognized, however, basaltic clasts and clinopyroxene crystals from the Miocene basaltic shield were reworked into the basin throughout the “volcanic hiatus.” Epiclastic particles from the shield are mostly represented by clinopyroxenes. It seems that these minerals are very resistant to weathering compared to basaltic lithic

fragments. Consequently, epiclastic processes (weathering and erosion) concentrated crystals, but a lot of information about the sources was lost by disappearance of volcanic lithics. Two different possibilities (or both together) can be invoked to explain the ubiquitous presence of the shield material: (1) the island was not completely covered by the ignimbrites and lava flows during the Mogán and Fataga volcanic phases, and (2) the Mogán and Fataga volcanic products were rapidly dissected by deep canyons, which cut into the shield rocks. The presence of alkaline syenite in the turbidites at the bottom of Unit III at Site 953 also suggests very rapid erosion in deep canyons reaching the cone sheet dike swarm within the Tejada caldera. Consequently, the geomorphological evolution of Gran Canaria was rapid during this erosional interval. Erosion rates on volcanoes can be very high and reach 0.1–1.0 m/k.y. (Young, 1969; Francis, 1983). Drake (1976) calculated erosion rates of 1–2 km/m.y. in the Chilean Andes. Absence of vegetation on Gran Canaria at the end of the Fataga volcanic period could also help speed up the erosion of the former volcanic formations. Moreover, this period of the “volcanic hiatus” is more humid than the late Pliocene and the Quaternary (Sarnthein et al., 1982; Stein, 1985; Tiedemann et al., 1989), so erosion could be higher during the moist period. However, the clastic fluxes during

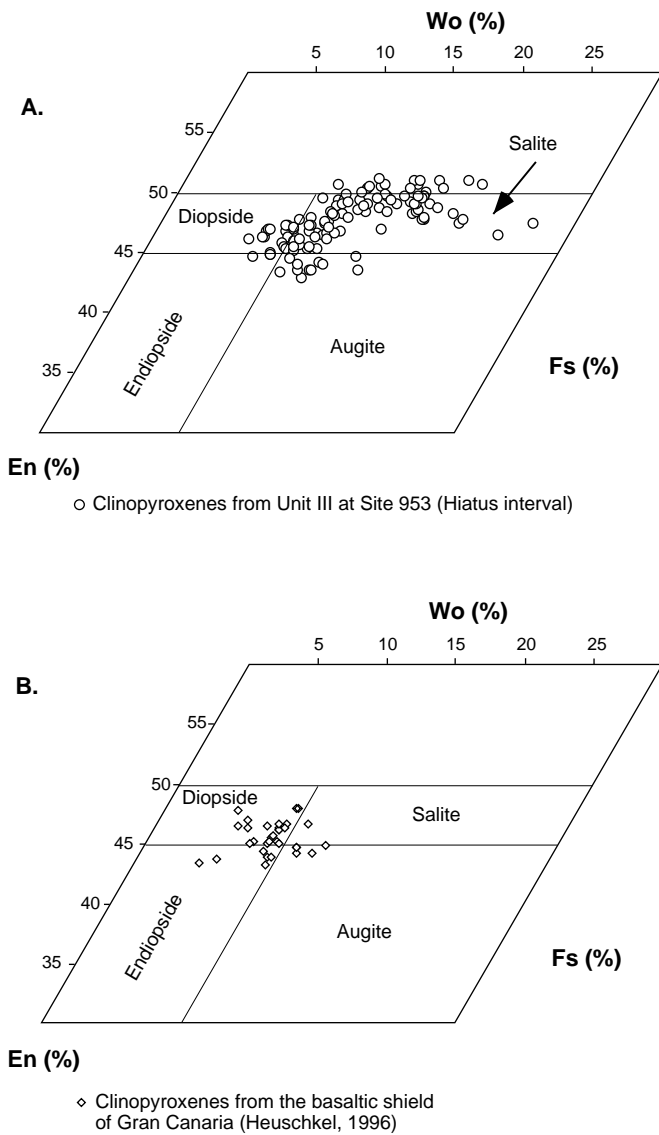


Figure 8. Clinopyroxene compositions in the wollastonite (Wo)-enstatite (En)-ferrosilite (Fs) diagram (after Poldervaart and Hess, 1951). **A.** Clinopyroxenes from the hiatus interval (Site 953). **B.** Clinopyroxenes from the Miocene basaltic shield (from Heuschkel, 1996).

this period are slow. This character is probably related to the fact that the deep barrancos, which correspond to the major areas of erosion, represent a small surface area, whereas other parts of the island could have been affected by soil development which slowed erosion.

The absence of quartz in the sediments of the “volcanic hiatus” strongly suggests the absence of submarine clastic influx from the northwestern African margin during the deposition of the entire sequence and is probably related to the presence of the topographic barrier between Gran Canaria and the island of Fuerteventura in the Miocene to Pliocene and that is still present (Amanay Bank). Moreover, eolian input from Africa is certainly very minor, except maybe for clay minerals such as chlorite and kaolinite. This is a major difference with the sediment provenances on the southern part of the apron (see Goldstrand, this volume).

The clastic input to the basin changes from Section 157-953C-15R-1 through the top of Unit III at Site 953. Volcaniclastic material (basaltic microlitic clasts, hydroclastic glass particles, and clinopyroxenes of different compositions) was deposited in the distal parts of

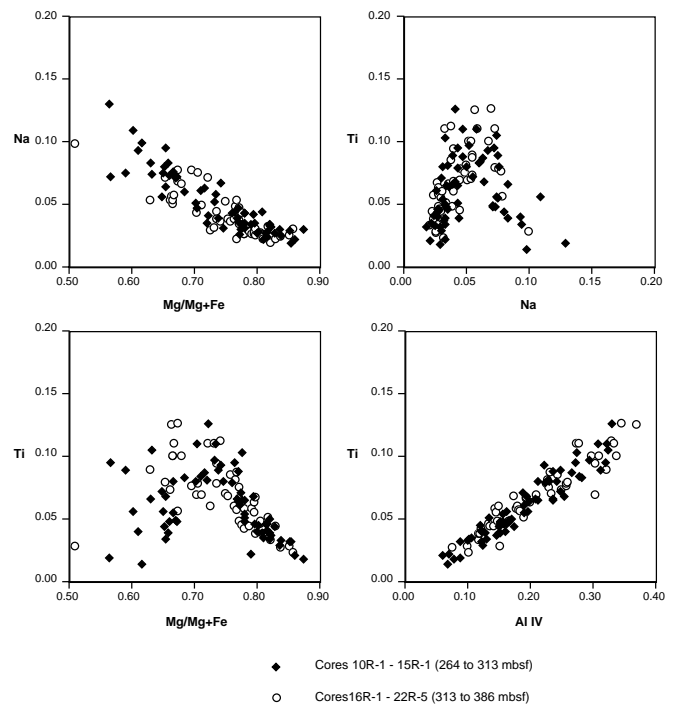


Figure 9. Binary element variation diagrams of the clinopyroxenes of the volcanic hiatus, Site 953.

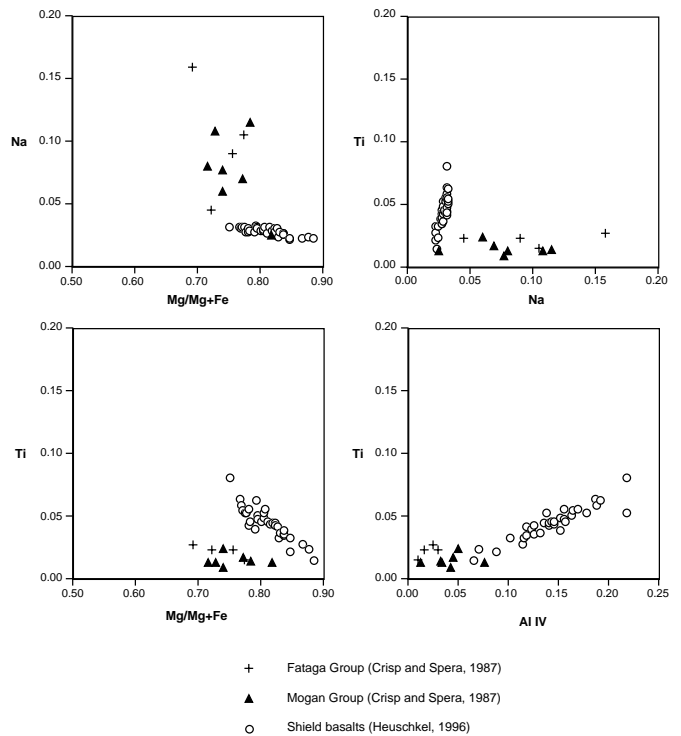


Figure 10. Binary element variation diagrams of the clinopyroxenes from Fataga and Mogán Groups (from Crisp and Spera, 1987), and from the Miocene basaltic shield of Gran Canaria (from Heuschkel, 1996).

Table 7. Representative compositions of clinopyroxenes in the basalts of the Miocene shield of Gran Canaria.*

Sample	1 Hes 94- 37-19	2 Hes 145- 54-2	3 Hes 94 40601-4-1	4 Hes 94 40601-2	5 Hes 122- 29-3	6 Hes 145- 28-3	7 Hes 145- 28-42	8 Hes 145- 28-14	9 Hes 95- 24-17
SiO ₂	47.84	49.17	48.94	50.08	51.54	50.72	50.99	49.51	50.58
TiO ₂	1.88	1.98	1.88	1.38	1.16	1.15	1.00	1.72	1.22
Al ₂ O ₃	5.20	5.04	4.29	3.93	2.54	3.15	2.85	4.17	3.02
Cr ₂ O ₃	0.60	0.55	0.24	0.51	0.39	0.48	0.57	0.35	0.58
FeO	6.90	6.07	8.02	5.81	5.36	5.86	4.63	6.57	5.72
MnO	0.16	0.12	0.06	0.09	0.12	0.11	0.08	0.12	0.08
MgO	14.96	14.01	14.93	15.86	16.11	15.74	16.78	15.07	16.20
CaO	21.28	21.93	20.76	21.61	22.14	21.81	22.14	21.28	21.25
Na ₂ O	0.41	0.43	0.38	0.36	0.31	0.33	0.31	0.39	0.37
Total	99.22	99.29	99.51	99.62	99.66	99.35	99.35	99.19	99.01
% Wo	47.88	47.98	45.55	46.56	46.36	45.10	45.04	44.83	43.99
% En	46.82	42.63	45.56	47.53	46.92	45.27	47.48	44.16	46.64
% Fs	5.31	9.39	8.88	5.91	6.72	9.63	7.48	11.01	9.36
Mg number	0.684	0.694	0.650	0.732	0.728	0.729	0.784	0.696	0.739
Al IV	0.217	0.168	0.177	0.151	0.100	0.115	0.113	0.151	0.117
Al VI	0.011	0.053	0.012	0.019	0.010	0.023	0.011	0.033	0.016
Ti + Cr	0.070	0.072	0.060	0.053	0.043	0.046	0.044	0.059	0.051
Ca + Na	0.879	0.907	0.856	0.880	0.896	0.892	0.900	0.880	0.874

Notes: * = from Heuschkel (1996). The structural formulas were calculated on the basis of six oxygens. Samples 1 and 2 are from the base of the basaltic shield in the northwest part of Gran Canaria. Samples 3 through 9 are from the southwest part of the island.

Table 8. Representative compositions of amphiboles in the silts and sands of Unit III, Site 953.

Core, section, interval (cm)	10R-3, 74-76	11R-4, 90-92	11R-4, 90-92	14R-2, 23-25	15R-1, 20-22
SiO ₂	38.64	39.05	38.34	53.45	38.66
TiO ₂	5.78	3.75	5.94	1.66	4.26
Al ₂ O ₃	12.82	12.54	13.59	1.46	12.90
FeO	13.59	16.63	10.68	9.25	17.06
NiO	0.32	0.46	0.11	0.96	0.55
MgO	10.81	9.91	12.32	17.52	9.31
CaO	12.03	11.38	11.73	4.96	11.33
Na ₂ O	2.91	2.73	2.35	6.43	2.80
K ₂ O	1.10	1.36	1.54	0.82	0.92
Total	98.00	97.81	96.60	96.51	97.79
Amphibole name	Kaersutite	Titanian-potassian- magnesian-hastingsite	Potassian-kaersutite	Richterit	Titanian-magnesian- hastingsite

Table 8 (continued).

Core, section, interval (cm)	15R-1, 20-22	18R-2, 72-74	19R-1, 97-99	20R-2, 32-34	22R-5, 80-82
SiO ₂	8.43	36.49	39.70	38.78	38.12
TiO ₂	7.01	5.71	5.94	4.11	4.04
Al ₂ O ₃	13.69	13.03	12.85	12.90	12.57
FeO	11.63	12.40	10.49	16.35	16.38
NiO	0.23	0.25	0.09	0.23	0.74
MgO	11.63	11.17	12.86	9.45	9.47
CaO	11.85	11.71	12.31	11.15	11.56
Na ₂ O	2.26	2.14	2.47	2.92	2.50
K ₂ O	1.18	1.28	0.94	1.25	1.41
Total	97.91	94.18	97.65	97.14	96.79
Amphibole name	Subsilicic kaersutite	Potassian-subsilicic kaersutite	Kaersutite	Titanian-ferroan-pargasite	Titanian-potassian- magnesian hastingsite

the submarine apron in addition to the epiclasts eroded from older volcanic formations. This material reflects the beginning of a new volcanic phase on Gran Canaria ~5.5 Ma (pre-Roque Nublo volcanic phase). Evidence for contemporary beginning of the pre-Roque Nublo volcanic phase is supported on land by petrologic and geochronological studies (McDougall and Schmincke, 1977; Pérez-Torrado et al., 1995). However, the presence of hydroclastic material suggests that the volcanic activity was at least partly subaqueous.

Interpretation of Paleontological Data

Turbidity currents are composed of material carried from their sources and also various amounts of material incorporated during

their transit down the slope to their sites of deposition. Hence, benthic foraminifers from turbidites typically include specimens from several depth zones ranging from the source area to greater depths. The depth of the source area and the nature of the pathway can be inferred from both the shallowest and the most abundant foraminifer assemblages present in the turbidites.

Volcaniclastic turbidites from the volcanic hiatus interval are dominated by an upper bathyal assemblage of benthic foraminifers with only trace amounts of other depth sensitive taxa including those from the shelf. This implies that the turbidites must have picked up very little debris from the shelf, perhaps because the shelf was shallow and narrow at this time. However, the volcaniclastic turbidites picked up a lot of foraminifers from the upper bathyal zone, suggest-

ing that the depth zone may have been a sediment reservoir or, at least, that the depth zone was extensive enough to allow production of large numbers of upper bathyal foraminifers that could be incorporated into volcanoclastic turbidites as they passed through to the basin.

We observed a distinct difference in benthic foraminifer assemblages in the late Pliocene and Quaternary turbidites compared to those of the volcanic hiatus. Turbidite faunas included shelf dwelling taxa in two distinct assemblages: one neritic assemblage with abundant miliolids and textularids from a clastic-starved shelf and one shelf to upper bathyal assemblage from a clastic-rich shelf and upper slope (assemblage from 0 to 1000 m). This suggests that there were two contrasting environmental settings that produced different foraminifer assemblages in turbidites during the late Pliocene and Quaternary. We suggest that sea level was largely responsible for these two end-member conditions. Beginning in the late Pliocene at ~3 Ma, intensification of glacial cycles produced large changes in sea level that increased from 10 to 40 m in the early Pliocene (Raymo et al., 1989; see also Tiedemann et al., 1994) to ~120 m in the Quaternary (Ruddiman et al., 1989). The early Pliocene shelf was shallow and narrow because of the small change in sea level, but the Quaternary shelf was wide and deep.

We propose that during Quaternary lowstands of the sea, the subaqueous island shelf was narrow and shallow, and volcanoclastic material passed quickly over the narrow shelf to the upper slope much as it did during the late Miocene and early Pliocene. However, during high stands of the sea, epiclastic material was trapped in the coastal zone for some time allowing a bryozoan reef community, including miliolid and textularid benthic foraminifers, to colonize the shelf, which was now wide and deep (Brunner et al., 1996). The biogenic carbonate material was the source of turbidite debris during the high stand of the sea until volcanoclastic material filled the coastal zone and spread across the shelf. Clastic starvation of the shelf was probably aided by the onset of arid climate in the region at ~2.8 Ma (Sarnthein et al., 1982; Stein, 1985; Tiedemann et al., 1989; Brunner and Miscalco, this volume).

It is interesting to reconsider the effects of sea-level change during the latest Miocene and earliest Pliocene. A wide range of evidence from sequence stratigraphy to oxygen isotopic analysis suggests that sea level varied with changes in ice volume at this time and resulted in changes in delivery of clastic materials to continental margins around the world (e.g., Haq et al., 1988). Sea level in the latest Miocene and earliest Pliocene fluctuated by about one third the magnitude of Quaternary cycles based on oxygen isotopic analysis (Hodell et al., 1986), beginning soon after 6 Ma with intense events at ~5.2 and 4.8 Ma (Hodell et al., 1989; Keigwin, 1987).

These sea-level events should have affected sedimentation at Gran Canaria, but the evidence is not clear in our data. There is an increase in sedimentation rate from 22 m/m.y. to 50 m/m.y. at 6 Ma (Brunner et al., this volume), but this could be in part caused by the onset of pre-Roque Nublo volcanism at ~5.5 Ma. There is no increase in neritic benthic foraminifers in turbidites to suggest a widening and deepening of the shelf and production of large numbers of neritic benthic foraminifers as in the late Pliocene and Quaternary.

Table 9. Proportions of benthic foraminifer suborders Miliolina, Textulariina, and Rotaliina in selected turbidites of Site 953.

Core, section, interval (cm)	Unit	Depth (mbsf)	Total	Miliolina	Textularia	Rotaliina
157-953A-						
1H-3, 88-90	I	3.88	323	22.9	7.46	9.7
2H-2, 22-24	I	9.32	401	22.7	2.2	75.1
4H-4, 79-81	I	31.89	335	35.8	9.0	55.2
8H-5, 28-30	I	70.88	407	18.9	5.7	75.4
9H-6, 114-116	I	82.74	396	1.3	1.8	97.0
11H-3, 38-40	I	96.48	330	1.2	0.6	98.2
12H-3, 28-30	I	105.89	250	0.8	0.0	99.2
13H-3, 17-19	I	115.27	348	33.9	6.6	59.5
14H-7, 25-27	I	130.85	370	0.5	0.8	98.6
16H-3, 5-7	I	143.66	26	0.0	0.0	100.0
16H-7, 20-22	I	149.80	330	9.1	1.5	89.4
18H-2, 87-89	I	161.97	394	0.3	0.0	99.7
18H-5, 132-134	I	166.93	33	0.0	0.0	100.0
20H-1, 22-24	I	178.82	326	0.3	0.6	99.1
10R-3, 74-78	III	267.46	53	1.9	0.0	98.1
11R-2, 144-148	III	276.36	2	0.0	0.0	100.0
15R-1, 20-22	III	312.31	50	0.0	0.0	100.0
15R-1, 100-102	III	313.11	20	0.0	0.0	100.0
18R-4, 58-61	III	345.70	161	0.0	0.0	100.0
19R-1, 97-99	III	351.18	614	0.0	0.0	100.0
20R-2, 12-14	III	361.43	331	0.0	0.0	100.0
22R-3, 89-91	III	383.00	372	0.3	1.1	98.7
24R-2, 129-131	IV	400.90	7	0.0	0.0	100.0
26R-4, 11-13	IV	421.92	14	0.0	0.0	100.0
31R-2, 145-148	IV	468.46	156	0.0	0.0	100.0

Note: Note the larger percentages of Miliolina and Textulariina in turbidites from 3.88, 9.32, 31.89, 70.88, 115.27, and 149.80 mbsf compared to those from other depths.

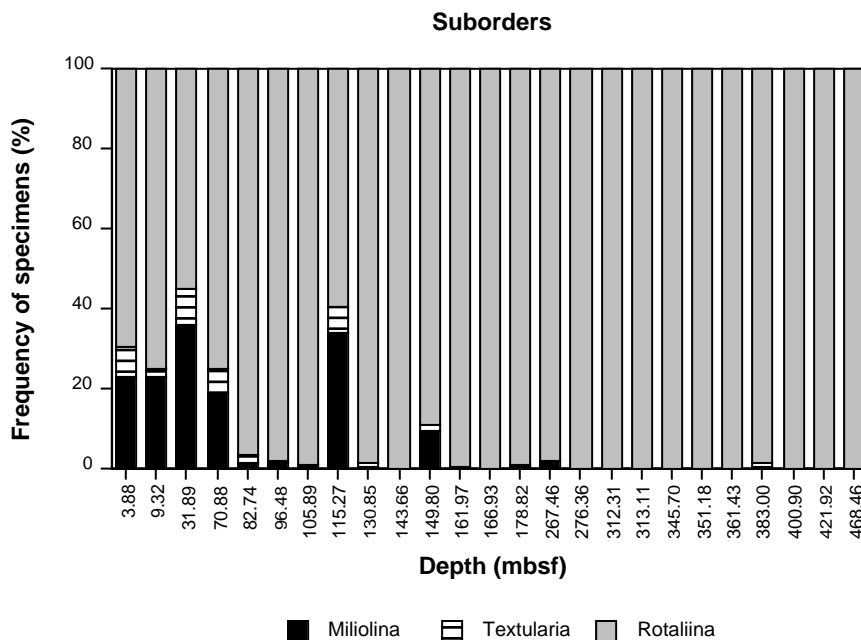


Figure 11. Stacked bar graph showing percentages of specimens in each of three suborders of benthic foraminifers, Site 953. The samples with large abundances of Miliolina and Textulariina are from biogenic carbonate turbidites and are characteristic of shelves starved of clastic sediments. Note that this type of turbidite occurs only above the top of the volcanic hiatus at 264 mbsf.

Residence Times of the Clastic Material on the Island's Shelf

Micropaleontologic data suggest short clastic storage times on the island shelf during the "volcanic hiatus," based on the near absence of shelf-dwelling foraminifers in the turbiditic deposits. Shelf development around Gran Canaria during this period was probably minor. Surprisingly, the major falls in sea level known from the latest Miocene and earliest Pliocene (see discussion above) are not recorded in the sediments from the "volcanic hiatus." However, if shelves developed during this interval, the storage of clastic material on shelves remained very short. Throughout the "volcanic hiatus," it appears that clastic material was either stored on the upper slope, where upper bathyal foraminifers were added to the volcanoclastic material before it was removed by turbidity currents, or was delivered directly from the subaerial fluvial system to the distal apron, picking up upper bathyal foraminifers during its transit across the upper slope. In either case, the rapid transit of clastic material from subaerial source to distal volcanic apron makes it an excellent recorder of the erosional history of the emergent part of the island.

Clastic material had a somewhat different pathway down the island margin during the late Pliocene and Quaternary period compared to the "volcanic hiatus" period. The numerous and large sea-level fluctuations during the late Pliocene and Quaternary induced development of broader and deeper shelves around the island than during the period of the volcanic hiatus. Such shelves were probably starved of clastic material during highstands of the sea, allowing bryozoan reefs to build up. In consequence, clastic material delivered to the deep basin was enriched in neritic carbonate debris swept from the shelf. In contrast, turbidity currents originated on the upper slope during Quaternary lowstands of the sea, and were enriched in volcanoclastic material and upper bathyal foraminifers.

CONCLUSIONS

The study of the clastic sediments deposited at Sites 953 and 954 during the late Miocene–early Pliocene "volcanic hiatus" of Gran Canaria on the northern part of the submarine volcanoclastic apron allows the reconstruction of the evolution of a volcanic island during a nonvolcanic period. Figure 12 summarizes the characteristics of the sedimentation and differences with eruptive periods. The following concluding remarks can be proposed:

1. Sedimentation rates during this period were minimal because of wide dispersal on the submarine apron of the eroded clastic material from the emergent part of the island.
2. Volcanoclastic material was emplaced by low-density turbidity currents on the northern flank of the submarine apron of Gran Canaria. Some turbidite emplacement was related to the dynamics of the fluvial system in barrancos of the emergent part of the island.
3. Modal and geochemical analyses of clinopyroxenes in epiclastic sediments allow the reconstruction of the evolution of volcanic sources over time. Volcanic deposits of the Mogán and Fataga Groups were rapidly dissected, leading to the formation of deep canyons (barrancos). In these barrancos, the erosion level quickly reached the Miocene basaltic shield, and the cone sheet dike swarm of the Tejada caldera. Additionally, the Miocene basaltic shield in the subaerial domain of the island might not have been capped everywhere with the Mogán and Fataga volcanic Groups deposits.
4. Most of the clastic material deposited on the volcanoclastic apron is nearly contemporary with erosion of the source area on land, because of short residence time on narrow shelves around Gran Canaria. This conclusion is supported by the pa-

leontologic data, which show that turbidites contained only a few foraminifers picked up from the shelf, which was probably narrow and shallow, but picked up many foraminifers from the upper slope, which must have been extensive, during their passage to the distal volcanic apron.

5. The beginning of the pre-Roque Nublo volcanic phase around 5.5 Ma is reflected in the sedimentation by an increase of the influx of microlitic basalt clasts and hydroclastic glass particles suggesting submarine eruptions, and by a change in clinopyroxene compositions.

The study of marine epiclastic sedimentation on a volcanoclastic apron by multidisciplinary approaches allows the reconstruction of the erosional and geomorphologic evolution of an emergent volcanic sequence in the source area of a volcanic island.

ACKNOWLEDGMENTS

During Leg 157, the crew of the *JOIDES Resolution* and the Ocean Drilling Program engineering, operations, technical, and logistic personnel were very efficient, and we are very thankful. We gratefully acknowledge M. Bocquet, J. Carpentier, P. Dorn, F. Dujardin, D. Malengros, J. Marti, C. Mulier, N. Pernot, P. Recourt, and P. Rouze (University Lille) for technical assistance in the analyses of the samples and preparation of the manuscript. Special thanks go to M. Buatier, S. Carey, C. Lefèvre, J.L. Potdevin, M. Seyler, and A. Trentessaux for helpful discussions on analytical results. S. Heuschkel (GEOMAR, Kiel) kindly provided electron microprobe analyses of clinopyroxenes of basaltic lavas of the shield of Gran Canaria. We are grateful to Dr. U. von Rad and an anonymous reviewer for thorough reviews, which contributed significantly to improvement of the manuscript. This project was supported by grants from the INSU-Geosciences Marines (Paris) and the CNRS-URA 719 (Lille), and in part by a grant from the JOI U.S. Science Support Program to C.B. (IMS Contribution Number 0186).

REFERENCES

- Brunner, C.A., Kuttner, S., and Schneider, J.L., 1996. Neogene turbidite deposition in an island hot-spot setting in the Canary Islands: paleoenvironmental clues from benthonic foraminifers. *Geol. Soc. Am. Abstr. Progr.*, 28:A43–A44.
- Chamley, H., 1986. *Clay Sedimentology*: Berlin (Springer-Verlag).
- Crisp, J.A., and Spera, F.J., 1987. Pyroclastic flows and lavas of the Mogán and Fataga formations, Tejada volcano, Gran Canaria, Canary Islands: mineral chemistry, intensive parameters, and magma chamber evolution. *Contrib. Mineral. Petrol.*, 96:503–518.
- Drake, R.E., 1976. Chronology of Cenozoic igneous and tectonic events in the central Chilean Andes: latitudes 35°30' to 36°S. *J. Volcanol. Geotherm. Res.*, 1:265–284.
- Düringer, P., Paicheler, J.C., and Schneider, J.L., 1991. Un courant d'eau continu peut-il générer des turbidites? Résultats d'expérimentations analogiques. *Mar. Geol.*, 99:231–246.
- Ferriz, H., and Schmincke, H.-U., 1989. The Miocene cone sheet dike swarm of Gran Canaria, Canary Islands, Spain. *Eur. Sci. Found. Meet. on Canarian Volcanism*, Lanzarote, Spain: 142–144.
- Fisher, R.V., 1961. Proposed classification of volcanoclastic sediments and rocks. *Geol. Soc. Am. Bull.*, 72:1409–1414.
- , 1966. Rocks composed of volcanic fragments and their classification. *Earth-Sci. Rev.*, 1:287–298.
- Fisher, R.V., and Schmincke, H.-U., 1984. *Pyroclastic Rocks*: New York (Springer-Verlag).
- Fisher, R.V., and Smith, G.A., 1991. Volcanism, tectonics and sedimentation. *Spec. Publ.—Soc. Econ. Petrol. Mineral.*, 45:1–5.
- Folk, R.L., 1974. *Petrology of Sedimentary Rocks*. Austin, TX (Hemphill Publ.).
- Folk, R.L., and Ward, W.C., 1957. Brazos River Bar: a study in the significance of grain-size parameters. *J. Sediment. Petrol.*, 27:3–27.

- Francis, E.H., 1983. Magma and sediment, II: Problems of interpreting palaeovolcanics buried in the stratigraphic column. *J. Geol. Soc. London*, 129:621–641.
- Funck, T., 1995. Structure of the volcanic apron north of Gran Canaria deduced from reflection seismic, bathymetric and borehole data [Ph.D. dissert.]. Univ. Kiel.
- Gerbe, M.C., and Schmincke, H.U., 1996. Dépôts ignimbritiques témoins de la transition d'une série trachy-rhyolitique à une série trachy-phonolitique, Gran Canaria (Iles Canaries). *12° Reun. Sci. Terre*, abstr. vol., 77.
- Haake, F.W., 1980. Benthische Foraminiferen in Oberflächen-Sedimenten und Kernen des Ostatlantiks vor Senegal/Gambia (Westafrika). *"Meteor" Forschungsergeb. Reihe C*, C32:1–29.
- Haq, B.U., Hardenbol, J., and Vail, P.R., 1988. Mesozoic and Cenozoic chronostratigraphy and cycles of sea-level change. In Wilgus, C.K., Hastings, B.S., Kendall, C.G.St.C., Posamentier, H.W., Ross, C.A., and Van Wagoner, J.C. (Eds.), *Sea-Level Changes—An Integrated Approach*. Spec. Publ.—Soc. Econ. Paleontol. Mineral., 42:72–108.
- Heuschkel, S., 1996. The Miocene shield basalts from Gran Canaria, Canary Islands: petrogenetic modeling of the evolution of a shieldstage in the Atlantic based on volcanological and geochemical data [Ph.D. thesis]. Univ. Kiel.
- Hodell, D.A., Benson, R.H., Kennett, J.P., and Rakic, K.E.B., 1989. Stable isotope stratigraphy of late Miocene-early Pliocene sequences in north-west Morocco: the Bou Regreg Section. *Paleoceanography*, 4:467–482.
- Hodell, D.A., Elmsstrom, K.M., and Kennett, J.P., 1986. Latest Miocene benthic $\delta^{18}\text{O}$ changes, global ice volume, sea level and the "Messinian salinity crisis." *Nature*, 320:411–414.
- Holtzapffel, T., 1985. Les minéraux argileux: préparation, analyse diffractométrique et détermination. *Mem. Soc. Geol. Nord.*, 12.
- Keigwin, L.D., 1987. Toward a high-resolution chronology for latest Miocene paleoceanographic events. *Paleoceanography*, 2:639–660.
- Leake, B.E., 1978. Nomenclature of amphiboles. *Am. Mineral.*, 63:1023–1052.
- Lietz, J., and Schmincke, H.-U., 1975. Miocene-Pliocene sea-level changes and volcanic phases on Gran Canaria (Canary Islands) in the light of new K-Ar ages. *Palaeogeogr., Palaeoclimatol., Palaeoecol.*, 18:213–239.
- Loizeau, J.L., Arbouille, D., Santiago, S., and Vernet, J.P., 1994. Evaluation of a wide range laser diffraction grain size analyser for use with sediments. *Sedimentology*, 41:353–361.
- Lutze, G.F., 1980. Depth distribution of benthic foraminifera on the continental margin off NW Africa. *"Meteor" Forschungsergeb. Reihe C*, 32:31–80.
- Lutze, G.F., and Coulbourn, W., 1984. Recent benthic foraminifera from the continental margin of Northwest Africa: community structure and distribution. *Mar. Micropaleontol.*, 8:361–401.
- Mathieu, R., 1971. Les associations de foraminifères du plateau continental atlantique du Maroc au large de Casablanca. *Rev. Micropaléontol.*, 14:55–61.
- , 1988. Foraminifères actuels et résurgences côtières sur la marge continentale Atlantique du Maroc. *Rev. Paleobiol.* (spec. vol.), 2:845–850.
- McDougall, I., and Schmincke, H.-U., 1977. Geochronology of Gran Canaria, Canary Islands: age of shield-building volcanism and other magmatic phases. *Bull. Volcanol.*, 40:1–21.
- Menard, H.W., 1956. Archipelagic aprons. *AAPG Bull.*, 40:2195–2210.
- Murray, J.W., 1991. *Ecology and Palaeoecology of Benthic Foraminifera*: London (Longman).
- Mutti, E., 1992. *Turbidite Sandstones*: Milan (Agip S.p.A., S. Donato Milanese).
- Patterson, R.T., and Fishbein, E., 1989. Re-examination of the statistical methods used to determine the number of point counts needed for micro-paleontological quantitative research. *J. Paleontol.*, 63:245–248.
- Pérez-Torrado, F.J., Carracedo, J.C., and Mangas, J., 1995. Geochronology and stratigraphy of the Roque Nublo Cycle, Gran Canaria, Canary Islands. *J. Geol. Soc. London*, 152:807–818.
- Poldervaart, A., and Hess, H.H., 1951. Pyroxenes in the crystallization of basaltic magma. *J. Geol.*, 59:472–489.
- Raymo, M.E., Ruddiman, W.F., Backman, J., Clement, B.M., and Martinson, D.G., 1989. Late Pliocene variation in Northern Hemisphere ice sheets and North Atlantic deep water circulation. *Paleoceanography*, 4:413–446.
- Ruddiman, W.F., Raymo, M.E., Martinson, D.G., Clement, B.M., and Backman, J., 1989. Pleistocene evolution: Northern Hemisphere ice sheets and North Atlantic Ocean. *Paleoceanography*, 4:353–412.
- Sarnthein, M., Theide, J., Pflaumann, U., Erlenkeuser, H., Fütterer, D., Koopmann, B., Lange, H., and Seibold, E., 1982. Atmospheric and oceanic circulation patterns of northwest Africa during the past 25 million years. In von Rad, U., Hinz, K., Sarnthein, M., and Seibold, E. (Eds.), *Geology of the Northwest African Continental Margin*: Berlin (Springer), 545–603.
- Schmincke, H.U., 1967. Cone sheet swarm, resurgence of Tejeda caldera, and the early geologic history of Gran Canaria. *Bull. Volcanol.*, 31:153–162.
- , 1969. Ignimbrite sequence on Gran Canaria. *Bull. Volcanol.*, 33:1199–1219.
- , 1976. The geology of the Canary Islands. In Kunkel, G. (Ed.), *Biogeography and Ecology in the Canary Islands*: The Hague (W. Junk), 67–184.
- , 1982. Volcanic and chemical evolution of the Canary Islands. In von Rad, U., Hinz, K., Sarnthein, M., and Seibold, E. (Eds.), *Geology of the Northwest African Continental Margin*: Berlin (Springer), 273–306.
- , 1994. *Geological Field Guide: Gran Canaria* (6th ed.): Kiel, Germany (Pluto Press).
- Schmincke, H.-U., and von Rad, U., 1979. Neogene evolution of Canary Island volcanism inferred from ash layers and volcanoclastic sandstones of DSDP Site 397 (Leg 47A). In von Rad, U., Ryan, W.B.F., et al., *Init. Repts. DSDP*, 47 (Pt. 1): Washington (U.S. Govt. Printing Office), 703–725.
- Shanmugam, G., Spalding, T.D., and Rofheart, D.H., 1993. Traction structures in deep-marine, bottom-current-reworked sands in the Pliocene and Pleistocene, Gulf of Mexico. *Geology*, 21:929–932.
- Shipboard Scientific Party, 1995a. Site 953. In Schmincke, H.-U., Weaver, P.P.E., Firth, J.V., et al., *Proc. ODP, Init. Repts.*, 157: College Station, TX (Ocean Drilling Program), 317–394.
- , 1995b. Site 954. In Schmincke, H.-U., Weaver, P.P.E., Firth, J.V., et al., *Proc. ODP, Init. Repts.*, 157: College Station, TX (Ocean Drilling Program), 395–431.
- Stein, R., 1985. Late Neogene changes of paleoclimate and paleoproductivity off Northwest Africa (DSDP Site 397). *Palaeogeogr., Palaeoclimatol., Palaeoecol.*, 49:47–59.
- Tiedemann, R., Sarnthein, M., and Shackleton, N.J., 1994. Astronomic timescale for the Pliocene Atlantic $\delta^{18}\text{O}$ and dust flux records of Ocean Drilling Program Site 659. *Paleoceanography*, 9:619–638.
- Tiedemann, R., Sarnthein, M., and Stein, R., 1989. Climatic changes in the western Sahara: aeolo-marine sediment record of the last 8 million years. In Ruddiman, W., Sarnthein, M., et al., *Proc. ODP Sci. Results*, 108: College Station, TX (Ocean Drilling Program), 241–277.
- Van den Bogaard, P., Schmincke, H.U., Freundt, A., Hall, C.M., and York, D., 1988. Eruption ages and magma supply rates during the Miocene evolution of Gran Canaria. *Naturwissenschaften*, 75:616–617.
- Wass, S.Y., 1979. Multiple origin of clinopyroxenes in alkali basaltic rocks. *Lithos*, 12:122–132.
- White, A.J.R., 1964. Clinopyroxenes from eclogites and basic granulites. *Am. Mineral.*, 49:883–888.
- Young, A., 1969. Present rate of land erosion. *Nature*, 224:851–852.

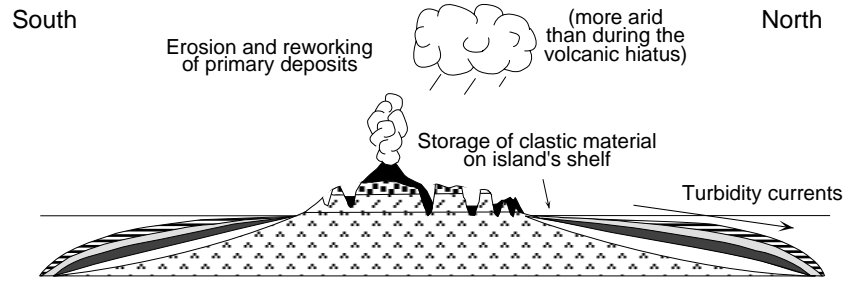
Date of initial receipt: 7 August 1996

Date of acceptance: 28 April 1997

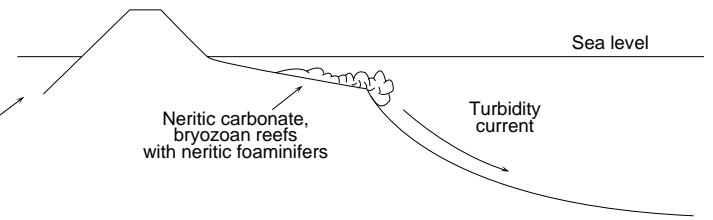
Ms 157-120

**CLASTIC INFLUXES AND SEDIMENTATION
ON THE VOLCANICLASTIC APRON OF GRAN CANARIA**

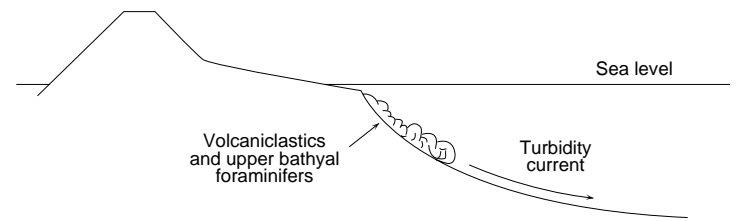
Pliocene - Pleistocene Roque Nublo Group (and post-Roque Nublo)



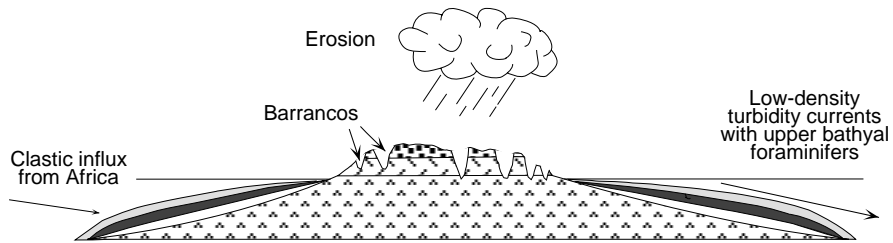
HIGH STAND PERIOD



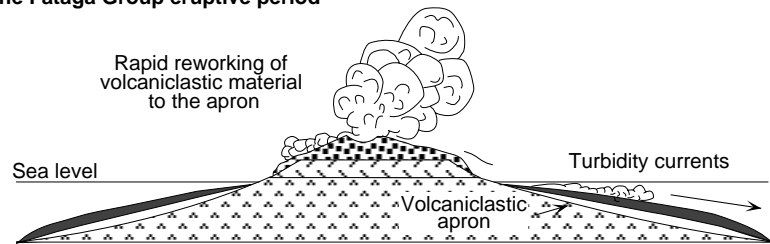
LOW STAND PERIOD



Late Miocene - early Pliocene volcanic hiatus (epiclastic sedimentation)



Miocene Fataga Group eruptive period



(not at scale)

- | | | | |
|---|-------------------|---|----------------|
|  | Roque Nublo Group |  | Units I and II |
|  | Fataga Group |  | Unit III |
|  | Mogan Group |  | Unit IV |
|  | Basaltic shield |  | Older Units |

Figure 12. Sketch of the sedimentary evolution on the volcaniclastic apron of Gran Canaria during eruptive and noneruptive periods, and relationships between sea-level fluctuations and shelf development.

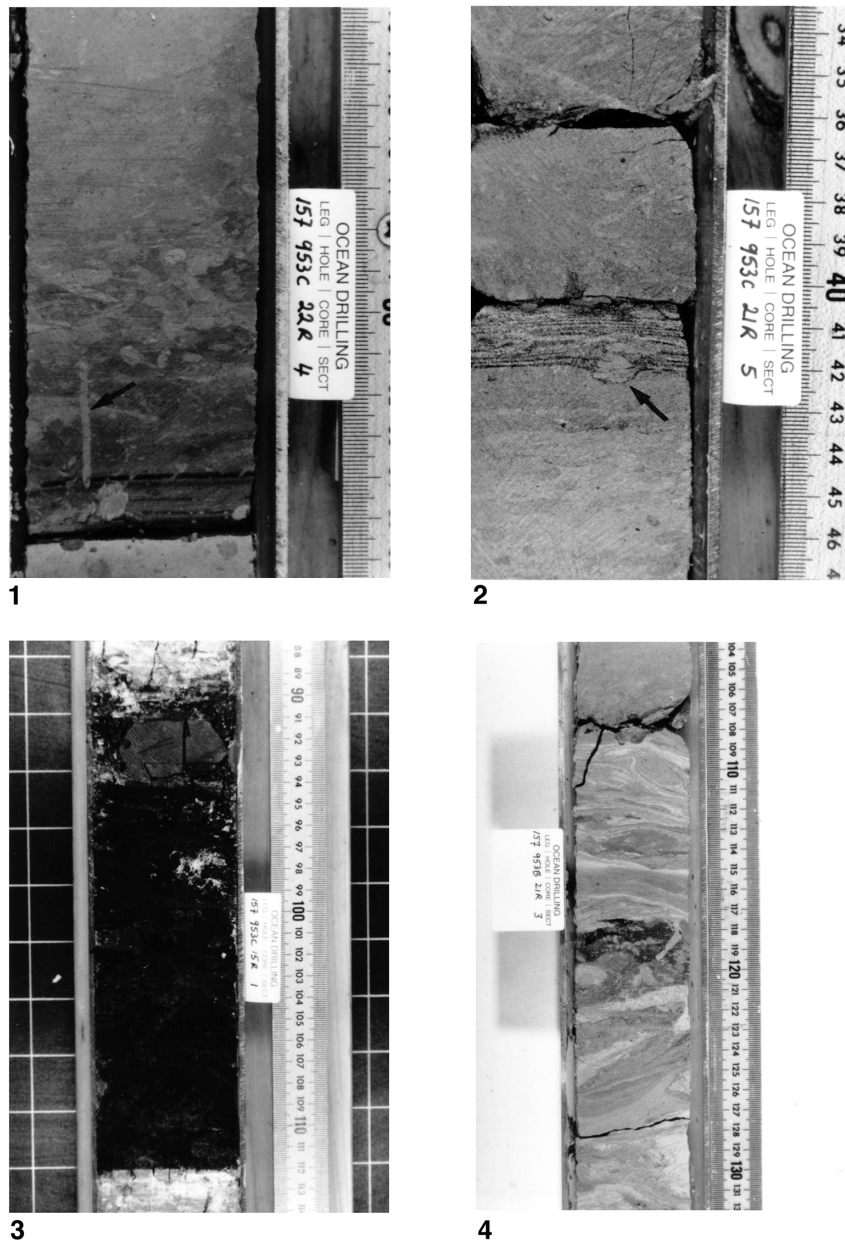


Plate 1. Turbidite sequences and soft-sediment deformation. **1.** Thin amalgamated turbidite layers. At the top, the hemipelagic nannofossil chalk is strongly bioturbated. Arrow = the vertical burrow crossing a turbidite layer (Sample 157-953C-22R-4, 72–87 cm). **2.** Arrow = thin planar-laminated turbidite sequence with load-casted ripples (Sample 157-953C-21R-5, 33–47 cm). **3.** Dark volcaniclastic turbidite sequence with fine-grained, 4-cm-thick, top layer (Sample 157-953C-15R-1, 87–114 cm). **4.** Soft-sediment deformation. In the middle of the photograph, sediments are brecciated (Sample 157-953C-21R-3, 103–133 cm).

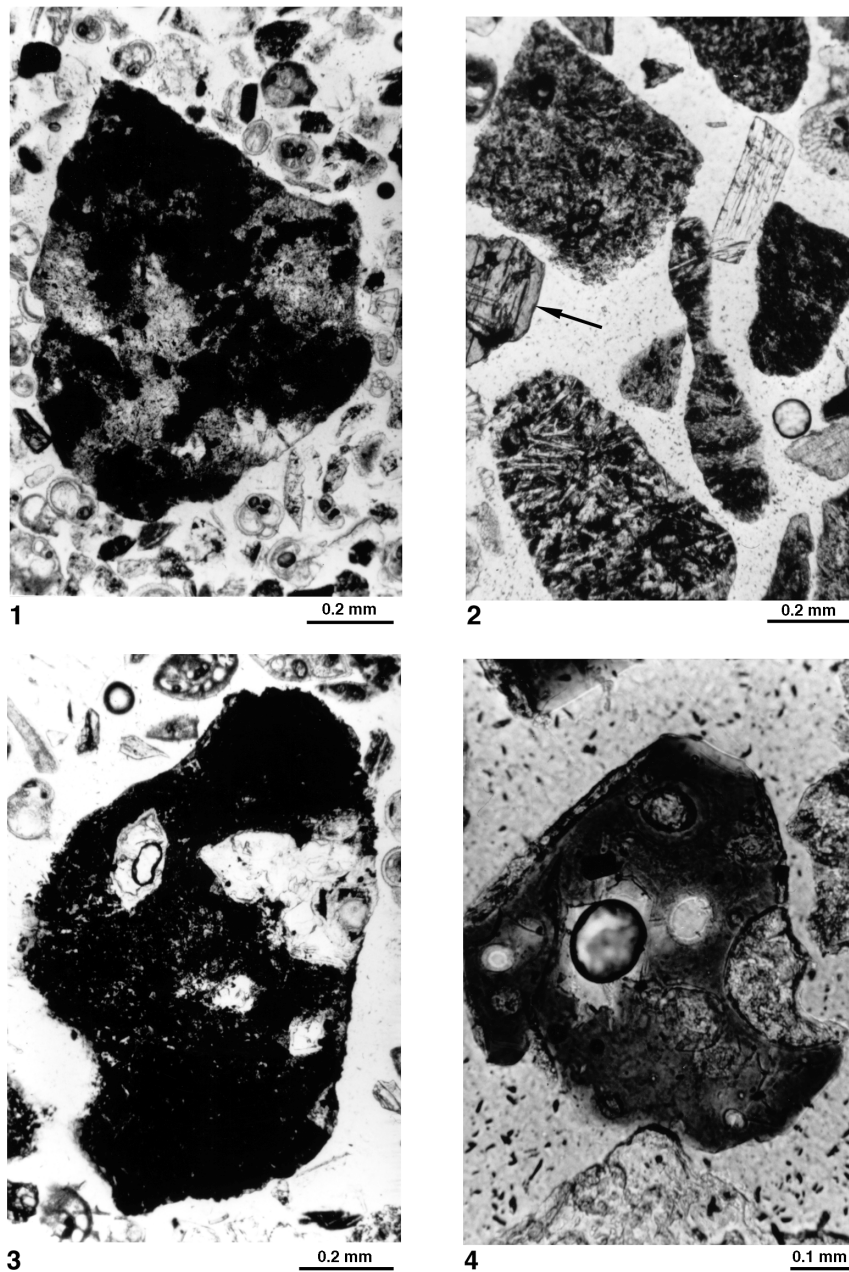


Plate 2. Photomicrographs of the sediments of the main volcanic hiatus (all plane-polarized light). **1.** Clast of ignimbrite with oxides patches within the groundmass (Fataga Formation; Sample 157-953C-18R-4, 58–61 cm; scale bar = 0.2 mm). **2.** Rounded trachyphonolitic clasts (Fataga Formation) and crystals (arrow = clinopyroxene; Sample 157-953C-20R-2, 12–14 cm; scale bar = 0.2 mm). **3.** Dark microlitic basaltic clast including olivine phenocryst pseudomorphs (basaltic shield; Sample 157-953C-22R-3, 89–91 cm; scale bar = 0.2 mm). **4.** Blocky and slightly vesicular brown glass fragment (Sample 157-953C-15R-1, 100–105 cm; scale bar = 0.1 mm).